1

2

3

4

5

6

7 **FtsK is Critical for the Assembly of the Unique Divisome**

8 **Complex of the FtsZ-less *Chlamydia trachomatis***

9 **Authors: McKenna Harpring[1], Junghoon Lee[2], Guangming Zhong[3], Scot P. Ouellette[2], and**
10 **John V. Cox[1]***

11 Affiliations: Department of Microbiology, Immunology, and Biochemistry. University of
12 Tennessee Health Science Center. Memphis, TN, USA[1], Department of Pathology,
13 Microbiology, and Immunology, University of Nebraska Medical Center, Omaha, NE, USA[2],
14 Department of Microbiology, Immunology, and Molecular Genetics, University of Texas Health
15 San Antonio, TX, USA[3]

16 *** Correspondence:**
17 Corresponding Author: John V. Cox
18 jcox@uthsc.edu

19

20 **Abstract:**

21 *Chlamydia trachomatis* serovar L2 *(Ct),* an obligate intracellular bacterium that does not encode

22 FtsZ, divides by a polarized budding process. In the absence of FtsZ, we show that FtsK, a

23 chromosomal translocase, is critical for divisome assembly in *Ct*. Chlamydial FtsK forms

24 discrete foci at the septum and at the base of the progenitor mother cell, and our data indicate

25 that FtsK foci at the base of the mother cell mark the location of nascent divisome complexes

26 that form at the site where a daughter cell will emerge in the next round of division. The

27 divisome in *Ct* has a hybrid composition, containing elements of the divisome and elongasome

28 from other bacteria, and FtsK is recruited to nascent divisomes prior to the other chlamydial

29 divisome proteins assayed, including the PBP2 and PBP3 transpeptidases, and MreB and MreC.

30 Knocking down FtsK prevents divisome assembly in *Ct* and inhibits cell division and septal

31 peptidoglycan synthesis. We further show that MreB does not function like FtsZ and serve as a

32 scaffold for the assembly of the *Ct* divisome. Rather, MreB is one of the last proteins recruited to

33 the chlamydial divisome, and it is necessary for the formation of septal peptidoglycan rings. Our

34 studies illustrate the critical role of chlamydial FtsK in coordinating divisome assembly and

35 peptidoglycan synthesis in this obligate intracellular bacterial pathogen.

36
37 **Word count: 221**

Introduction

Most bacteria divide by a highly conserved process termed binary fission, which occurs through the symmetric division of the parental cell into two daughter cells (Harpring 2023). However, *Chlamydia trachomatis* serovar L2 (*Ct*), a coccoid, gram-negative, obligate intracellular bacterium divides by a polarized cell division process characterized by an asymmetric expansion of the membrane from one pole of a coccoid cell resulting in the formation of a nascent daughter cell (Abdelrahman 2016; Ouellette SP 2022).

Ct undergoes a biphasic developmental cycle during infection. Non-replicating and infectious elementary bodies (EBs) bind to and are internalized by target cells. Following internalization, EBs within a membrane vacuole, termed the inclusion, differentiate into replicating reticulate bodies (RBs). After replication, RBs undergo secondary differentiation into EBs, which are released from cells to initiate another round of infection (Abdelrahman 2005).

In evolving to obligate intracellular dependence, *Ct* has eliminated several gene products essential for cell division in other bacteria, including the central coordinator of divisome formation, FtsZ (Stephens 1998; Ouellette SP 2020). This tubulin-like protein forms filaments that associate to form a ring at the division plane (Barrows 2021), which serves as a scaffold for the assembly of the other components of the bacterial divisome that regulate the processes of septal peptidoglycan (PG) synthesis and chromosomal translocation. Of the twelve divisome proteins shown to be essential for cell division in the model gammaproteobacterial organism, *E. coli, Ct* encodes homologues of FtsK, a chromosomal translocase (Ouellette SP 2012); FtsQLB, regulators of septal PG synthesis (Ouellette SP 2015; Kaur 2022), FtsW, a septal transglycosylase (Putman T 2019), and penicillin binding protein 3 (PBP3/FtsI), a septal transpeptidase (Ouellette SP 2012).

61   In addition to the divisome, rod-shaped bacteria employ another multiprotein complex, the

62   elongasome, which directs sidewall PG synthesis (Liu 2020) necessary for cell lengthening and

63   the maintenance of cell shape prior to division. Although *Ct* is a coccoid organism, it encodes

64   several elongasome proteins, including MreB, MreC, RodA, RodZ, and penicillin binding

65   protein 2 (PBP2), a sidewall transpeptidase (Ouellette SP 2012; Ouellette SP 2014; Cox 2020).

66   The actin-like protein MreB is essential for cell division (Ouellette SP 2012; Abdelrahman 2016)

67   and forms septal rings in *Ct* (Kemege 2015; Liechti 2016; Lee 2020). These observations led to

68   the proposal that MreB replaces FtsZ in *Ct* and serves as a scaffold necessary for the assembly of

69   the chlamydial divisome (Lee 2020).

70   While inhibitor studies suggest that chlamydial cell division is dependent upon elements of

71   the divisome and elongasome from other organisms (Ouellette SP 2012; Abdelrahman 2016; Cox

72   2020), the composition and ordered assembly of the chlamydial divisome and its distribution

73   during polarized budding are undefined. We hypothesized that FtsK, a chromosomal translocase,

74   serves a critical function in regulating the division process of *Ct,* given previous observations

75   demonstrating it interacts with elements of both the elongasome and divisome (Ouellette SP

76   2012). We show here that FtsK is critical for the assembly of the hybrid divisome complex of *Ct*

77   and that MreB does not serve as a scaffold necessary for the assembly of the chlamydial

78   divisome. Rather, chlamydial MreB associates with this hybrid divisome complex late in the

79   chlamydial divisome assembly process, and MreB filament formation is necessary for the

80   formation of septal PG rings. Therefore, our data identify FtsK as a key regulator of the cell

81   division process of *Ct*.

82

Results

FtsK Forms Foci in *Ct* that Mark the Location of Divisome Complexes

In the *E. coli* linear divisome assembly pathway (Du 2017), FtsK is the first protein downstream of FtsZ encoded by *Ct* (Figure 1A). In other organisms, FtsK is uniformly distributed at the septum of dividing cells (Yu 1998; Wang 2006; Veiga 2017). To investigate the localization of FtsK during cell division in *Ct*, HeLa cells were infected with *Ct*. To overcome the challenges associated with assessing cell morphologies in densely packed inclusions in infected cells, we analyzed FtsK localization in *Ct* derived from lysates of infected HeLa cells at 21 hrs post-infection (hpi) as described previously (Ouellette SP 2022). *Ct* were stained with an antibody against the chlamydial major outer membrane protein (MOMP) and an antibody that recognizes endogenous FtsK. Blotting analysis revealed that this FtsK antibody recognizes a single protein with the predicted molecular mass of FtsK (Supp. Fig. S1A). Our results showed that, unlike FtsK in other organisms, chlamydial FtsK accumulates in discrete foci in the membrane of coccoid cells (Fig. 1B). In cell division intermediates, FtsK localized in foci at the septum, foci at the septum and at the base of the progenitor mother cell, or foci at the base of the progenitor mother cell only (Figure 1C). The chlamydial FtsK foci observed during cell division were not uniformly distributed at the septum, rather septal foci of FtsK were restricted to one side of the MOMP-stained septum. In addition, the FtsK foci were often above or below (marked with arrowheads in Fig. 1C) the MOMP-stained septum. Similar analyses were performed using

102   *Ct* transformed with the pBOMB4-Tet (-GFP) plasmid encoding FtsK with a C-terminal

103   mCherry tag. The expression of this mCherry fusion is under the control of an

104   anhydrotetracycline (aTc)-inducible promoter. HeLa cells were infected with the transformant,

105   and the expression of the fusion was induced by the addition of 10nM aTc to the media of

106   infected cells at 19hpi. RBs were harvested from the induced cells at 21hpi and stained with

107   MOMP antibodies. Imaging analyses revealed that like endogenous FtsK, FtsK-mCherry

108   accumulated in foci in coccoid cells (Fig. 1D), and in division intermediates, it localized in foci

109   at the septum, foci at the septum and at the base of the progenitor mother cell, or foci at the base

110   of the progenitor mother cell only (Fig. 1E). The foci of FtsK-mCherry, like endogenous FtsK,

111   were often offset relative to the plane defined by MOMP staining at the septum (arrowhead in

112   Fig. 1E). Inclusion forming unit (IFU) assays demonstrated that overexpression of the FtsK-

113   mCherry fusion had no effect on chlamydial developmental cycle progression and the production

114   of infectious EBs (Supp. Fig. S2A). While it is possible that the population of FtsK at the base of

115   the mother cell is a remnant of FtsK from a previous division, ~20% of dividing cells have a

116   secondary bud (Fig. 1F), and FtsK and FtsK-mCherry accumulate in foci at the base of

117   secondary buds (arrowheads in Fig. 1G), suggesting that the population of FtsK at the base of the

118   mother cell corresponds to a nascent divisome complex that forms at the site where the daughter

119   cell will arise in the next round of division.

120   To investigate the distribution of other putative chlamydial divisome components during

121   budding, we transformed *Ct* with plasmids encoding PBP2, PBP3, or MreC with an N-terminal

122   mCherry tag. IFU assays demonstrated that the aTc induced overexpression of the PBP2, PBP3,

123   and MreC fusions had no effect on the developmental cycle progression of *Ct* (Supp. Fig. S2A).

124   In addition, blotting analyses revealed that mCherry antibodies primarily detected single species

125   with the predicted molecular mass of the FtsK, PBP2, PBP3, and MreC fusions in lysates

126   prepared from induced cells (Supp. Fig. S1B). The PBP2, PBP3, and MreC fusions were induced

127   by the addition of 10nM aTc to infected cells at 19hpi, and the induced cells were harvested at

128   21hpi and stained with MOMP antibodies. Imaging analyses revealed that the PBP2, PBP3, and

129   MreC fusions accumulated in foci in coccoid cells (Fig. 2A), and in cell division intermediates,

130   the fusions accumulated in foci at the septum, in foci at the septum and at the base of the

131   progenitor mother cell, or in foci only at the base of the progenitor mother cell (Fig. 2B). Similar

132   analyses with an MreB_6xHis fusion (Lee 2020) revealed that MreB exhibited a similar

133   localization profile (Figs. 2A and B). Each of these fusions, like FtsK, were restricted to one side

134   and were often slightly above or slightly below (marked with arrowheads in Fig. 2B) the

135   MOMP-stained septum in dividing cells. The foci of the fusions were also detected at the base of

136   secondary buds (arrowheads in Supp. Fig. S2B). Quantification of the localization profiles of

137   endogenous FtsK and the various fusion proteins revealed that the distribution profile of FtsK-

138   mCherry accurately reflected the distribution of endogenous FtsK (Fig. 2C). Furthermore, a

139 greater percentage of FtsK was associated with the base of dividing cells (including cells with

140 septum and base, and cells with base alone) suggesting that FtsK associates with nascent

141 divisomes at the base of dividing cells prior to the other putative divisome proteins assayed.

142 Finally, this analysis suggested that MreB associated with nascent divisomes at the base of

143 dividing cells after mCherry-PBP2 and mCherry-PBP3 (marked with # in Fig. 2C). The

144 localization profiles of the chlamydial divisome proteins (Figs. 1 and 2) likely reflect the

145 assembly of divisome complexes at the septum and at the base of the progenitor mother cell, and

146 the disassembly of the septal divisome when divisome proteins are only present at the base of the

147 mother cell.

148 Since it was possible that the localization profiles of the mCherry-PBP2 and mCherry-PBP3

149 fusions were at least in part due to their induced over-expression, we performed similar studies

150 with rabbit antibodies generated against peptides derived from PBP2 or PBP3 (Ouellette SP

151 2012). Blotting analyses (Supp. Fig. S1C) with these antibodies revealed that they recognized

152 mCherry-PBP2 and mCherry-PBP3 in *Ct* lysates, and immunofluorescent staining with the PBP2

153 and PBP3-specific antibodies (Supp. Fig. S1D) completely overlapped the mCherry fluorescence

154 in cells when the mCherry PBP2 and PBP3 fusions were inducibly expressed in *Ct*. Imaging

155 analyses with the antibodies that recognize endogenous PBP2 and endogenous PBP3 indicated

156 that these antisera detected foci in coccoid cells, and in cell division intermediates, the PBP2 and

157 PBP3 antibodies detected foci at the septum, foci at the septum and at the base of the mother cell,

158   or foci at the base alone (Supp. Fig. S3A). Quantification revealed that the localization profiles

159   of endogenous PBP2 and PBP3 in division intermediates (Supp. Fig. S3B) were not statistically

160   different than the localization profiles observed for the mCherry fusions of PBP2 and PBP3 (Fig.

161   2C).

162   The quantification in Fig. 2C suggested that FtsK is recruited to nascent divisomes that form

163   at the base of dividing cells prior to the other divisome components assayed. This hypothesis was

164   tested by staining cells expressing the PBP2, PBP3, MreC, or MreB fusions with antibodies that

165   recognize endogenous FtsK. Imaging analyses revealed that in a subset of cells, FtsK was

166   detected in foci at the septum and at the base of dividing cells, while each of the fusions was only

167   detected at the septum where they overlapped the distribution of septal FtsK (Fig. 2D), indicating

168   that FtsK is recruited to nascent divisomes at the base of the cell prior to the other divisome

169   components assayed. Additional analyses revealed that FtsK also overlapped the distribution of

170   the PBP2, PBP3, MreC, and MreB fusions following their appearance at the base of dividing

171   cells (Supp. Fig. S4A). Quantification revealed the percentage of cells in which FtsK overlapped

172   the distribution of each of the fusions at the septum, at the septum and the base, and at the base

173   alone in division intermediates (Supp. Fig. S4B).

174   **MreB Filament Formation is not Required for Foci Formation by FtsK, PBP2, and PBP3**

175   MreB was one of the last components that associated with nascent divisomes forming at the

176   base of the progenitor mother cell (Fig. 2C). To investigate whether MreB filament formation

177 was required for the formation of foci by the other chlamydial divisome components, HeLa cells

178 were infected with *Ct* transformed with the FtsK, PBP2, PBP3, MreC, or MreB fusions, and the

179 fusions were induced by adding 10nM aTc to the media of the infected cells at 20hpi for 1hr.

180 During the induction period, cells were incubated in the absence (Figs. 3B and 3D) or presence

181 (Figs. 3C and 3E) of the MreB inhibitor, A22, which inhibits MreB filament formation (Bean,

182 2009). RBs were harvested at 21hpi and stained with the appropriate antibodies to assess the

183 effect of A22 on the cellular distribution of the fusions. As previously shown (Ouellette SP 2012;

184 Cox 2020), A22 inhibits chlamydial budding and most cells in the population were coccoid

185 following A22 treatment (Fig. 3A). Furthermore, approximately 50% of the untreated control

186 cells were coccoid, which is consistent with prior estimates of the number of non-dividing RBs at

187 this stage of the developmental cycle (Lee 2018), indicating that our lysis procedure does not

188 lead to a bias in the number of non-dividing coccoid cells in the population. MreB in coccoid

189 cells adopted a diffuse pattern of localization following A22 treatment (Fig 3). A22 also had a

190 statistically significant effect on the percent of coccoid cells containing MreC foci, but it did not

191 affect the ability of FtsK, PBP2, or PBP3 to form foci in coccoid cells (Figs. 3D and 3E). These

192 data indicate that MreB filaments do not function as a scaffold that is necessary for the assembly

193 of all divisome components in *Ct*.

194 **Effect of *ftsk* and *pbp2* Knockdown on Cell Division and Divisome Assembly in *Ct***

195 To further investigate the mechanisms that regulate divisome assembly in *Ct*, we inducibly

196 repressed the expression of *ftsK* or *pbp2* using CRISPRi technology, which has been used to

197 inducibly repress the expression of genes in *Ct* (Ouellette SP 2021). CRISPRi employs a

198 constitutively expressed crRNA that targets an inducible dCas enzyme (dCas12) to specific

199 genes where it binds but fails to cut, thus inhibiting transcription. We transformed *Ct* with the

200   pBOMBL12CRia plasmid that constitutively expresses an *ftsK* or *pbp2*-specific crRNA, which

201   target sequences in the *ftsK* or *pbp2* promoter regions. To determine whether *ftsK* and *pbp2*

202   transcript levels were altered using this CRISPRi approach, dCas12 expression was induced by

203   the addition of 5nM aTc to the media of infected cells at 8hpi. Control cells were not induced.

204   Nucleic acids were isolated from induced cells and uninduced control cells at various times, and

205   RT-qPCR was used to measure *ftsK* or *pbp2* transcript levels. This analysis revealed that the

206   induction of dCas12 resulted in ~10-fold reduction in *ftsK* transcript levels by 15hpi in cells

207   expressing the *ftsK*-targeting crRNA (Supp. Fig. S5A), and ~8-fold reduction in *pbp2* transcript

208   levels in cells expressing the *pbp2*-targeting crRNA (Supp. Fig. S5B), while these crRNAs had

209   minimal or no effect on chlamydial *euo* and *omcB* transcript levels, suggesting that the *ftsK* and

210   *pbp2* crRNAs specifically inhibit the transcription of *ftsK* and *pbp2* (Supp. Figs. S5A and S5B).

211   To investigate the effect of *ftsK* or *pbp2* down-regulation on developmental cycle progression,

212   dCas12 was induced by the addition of aTc to the media of infected cells at 4hpi. Control cells

213   were not induced. The cells were then fixed at 24hpi and stained with MOMP and Cas12

214   antibodies. Imaging analysis revealed that *Ct* morphology was normal and dCas12 was

215   undetectable in the inclusions of uninduced control cells, while foci of dCas12 were observed in

216   the induced cells, and *Ct* in the inclusion exhibited an enlarged aberrant morphology (Supp. Figs.

217   S5C and S5D), suggesting that the inducible knockdown of *ftsK* or *pbp2* blocks chlamydial cell

218   division. In additional studies, we induced dCas12 at 17hpi in cells expressing the *ftsK* or *pbp2*-

219   targeting crRNAs. Lysates were prepared and the cells were fixed at 21hpi, and localization

220   studies revealed that foci of endogenous FtsK and PBP2 were almost undetectable when *ftsK* or

221   *pbp2* were transiently knocked down using this CRISPRi approach (Supp. Fig. S5E).

222   To assess whether the knockdown of *ftsK* or *pbp2* arrests *Ct* division at a specific stage of

223   polarized budding, HeLa cells were infected with *Ct* transformed with the pBOMBL12CRia

224   plasmids encoding the *ftsK* or *pbp2*-targeting crRNAs. At 17hpi, dCas12 was induced by the

225   addition of 20nM aTc to the media. Control cells were not induced. RBs were harvested from

226   induced and uninduced control cells at 22hpi and stained with MOMP antibodies, and imaging

227   analyses quantified the division intermediates present in the population. These analyses revealed

228   that >60% of the *Ct* in the uninduced controls were at various stages of polarized budding (Figs.

229   4A and B), while ~90% of the cells were coccoid when *ftsK* was knocked down (Fig. 4A), and

230   ~85% of the cells were coccoid following *pbp2* knockdown (Fig. 4B), suggesting that the

231   initiation of polarized budding of *Ct* is inhibited when *ftsK* or *pbp2* are knocked down.

232   We next examined whether the knockdown of *ftsK* affected foci formation by PBP2 or PBP3

233   in coccoid cells. HeLa cells were infected with *Ct* transformed with the pBOMBL12CRia

234   plasmid encoding the *ftsK*-targeting crRNA. At 17hpi, dCas12 was induced by the addition of

235   10nM aTc to the media. Control cells were not induced. RBs were harvested from induced and

236   uninduced control cells at 22hpi, and the localization of endogenous PBP2 and PBP3 in coccoid

237   cells was assessed (Figs. 4C and 4D). This analysis revealed that the number of coccoid cells

238   with polarized foci of PBP2 and PBP3 were reduced by approximately 80% following *ftsK*

239   knockdown (Fig. 4E). In similar analyses, we assessed the effect of *pbp2* knockdown on the

240   ability of FtsK and PBP3 to form foci in coccoid cells. While FtsK retained its ability to form

241   foci in coccoid cells following *pbp2* knockdown, foci of PBP3 were almost entirely absent in

242   *pbp2* knockdown cells (Figs. 4C and 4D). Quantification of these assays revealed that FtsK is

243   necessary for foci formation by both the PBP2 and PBP3 transpeptidases, while PBP2 is

244   necessary for foci formation by PBP3 (Figs. 4E and 4F). Our data place FtsK upstream of, and

245   necessary for, the addition of PBP2 and PBP3 to the *Ct* divisome, and PBP2 upstream of and

246   necessary for the addition of PBP3 to the *Ct* divisome. These results are consistent with inhibitor

247   studies that indicated PBP2 acts upstream of PBP3 in the polarized budding process of *Ct* (Cox

248   2020).

249   To investigate whether the catalytic activity of PBP2 is necessary to maintain its association

250   with the *Ct* divisome, HeLa cells were infected with *Ct*, and mecillinam, an inhibitor of the

251   transpeptidase activity of PBP2 (Kocaoglu 2015; Cox 2020), was added to the media of infected

252   cells at 20hpi. Cells incubated in the absence of mecillinam were included as a control.

253   Mecillinam-treated and control cells were harvested at 22hpi and the effect of inhibiting the

254   catalytic activity of PBP2 on the localization of FtsK, PBP2, and PBP3 was determined. As

255   shown previously, mecillinam blocks chlamydial division (Ouellette SP 2012; Cox 2020), and

256   most cells in the population assumed a coccoid morphology (Fig. 5A). We then determined the

257   localization of endogenous FtsK, PBP2, and PBP3 in drug-treated and control coccoid cells.

258   Mecillinam treatment resulted in a ~50% reduction in the number of cells with polarized foci of

259   PBP2 (Figs. 5B - 5E). There was a similar reduction in polarized foci of PBP3 following

260   mecillinam treatment (Figs. 5B - 5E). These data indicate that the catalytic activity of PBP2 is

261   necessary for PBP2 to efficiently associate with or maintain its association with polarized

262   divisome complexes. Furthermore, consistent with *pbp2* knockdown studies, PBP3 association

263   with the divisome complex is dependent on the prior addition of PBP2 to the complex, but foci

264   formation by FtsK is unaffected when PBP2 foci are reduced in number (Fig. 5).

265   **Effect of Inhibitors and *ftsk* Knockdown on PG Organization in *Ct***

266   To assess the morphology of PG at the septum and the base of dividing cells, we used an

267   EDA-DA labeling strategy (Liechti 2014; Cox 2020). This approach enabled the detection of PG

268   foci, bars, and rings in dividing *Ct* (Liechti 2021). Our imaging analysis revealed that in some

269   instances PG foci were detected at both the septum and at the base of the progenitor mother cell

270   (Fig. 6A), and in other instances PG organization at the septum and the base differed. In the

271   example shown (Fig. 6B), a PG foci was detected at the septum while a PG ring was detected at

272   the base of the mother cell. In additional analyses, we compared the localization of mCherry-

273   PBP3 to the localization of PG in cells where the expression of this mCherry fusion had been

274   induced by the addition of aTc to the media. This analysis, which was restricted to PG formation

275   at the septum of dividing cells, revealed that multiple foci of PBP3 were associated with a septal

276   PG ring (Fig. 6C). Furthermore, the PG ring was at an angle relative to the MOMP-stained

277   septum. Similar analyses revealed that 2 foci of endogenous FtsK were associated with PG that

278   was again at an angle relative to the MOMP-stained septum. This was true even though the PG

279   had not fully reorganized into a ring structure (Fig. 6C).

280   We then determined the effect of A22 and mecillinam on PG synthesis/organization. Since

281   both of these drugs induce *Ct* to assume a coccoid morphology, we initially characterized PG

282   organization in untreated coccoid cells. We detected foci, bars, or rings in ~80% of untreated

283   coccoid cells (Figs. 6D and 6E), which make up ~50% of the cells in the inclusion at this stage of

284   the developmental cycle (Lee 2018). Furthermore, each of these PG intermediates exhibited a

285   polarized distribution in untreated coccoid cells (Fig. 6D). Although we cannot rule out that

286   continued PG synthesis and reorganization occurs in polarized division intermediates, PG rings

287   can arise prior to any of the morphological changes that occur during the polarized division of

288   *Ct.*

289   Prior studies have shown that inhibitors of MreB filament formation prevent the appearance

290   of PG-containing structures in *Ct* (Liechti 2014; Ouellette SP 2022). To assess whether MreB

291   filament formation is required for PG synthesis and/or PG reorganization, we infected HeLa cells

292   with *Ct*, and EDA-DA and A22 were added to the media of infected cells at 18hpi. The cells

293   were harvested at 22hpi, lysates were prepared, and PG localization was determined. These

294   analyses revealed that PG was diffuse/undetectable in the majority of A22-treated cells, and, in

295   those cells where PG was still detected, it could not convert into ring structures (Figs. 6E and

296   6F). In similar experiments, we assessed the effect of mecillinam on the appearance of PG

297   intermediates in coccoid cells. These analyses revealed that PG formed discrete foci or bars in

298   60% of mecillinam-treated cells (Figs. 6E and 6F). However, these PG intermediates could not

299   convert into PG rings when the transpeptidase activity of PBP2 was inhibited. Finally, we

300   assessed PG organization in cells where *ftsK* was knocked down by inducing dCas12 in the *ftsK*

301   knockdown strain by the addition of aTc to the media of infected cells at 17hpi. Cells were fixed

302   at 21hpi, and localization studies revealed that *ftsK* knockdown had the most dramatic effect on

303   PG localization, which was diffuse/undetectable in ~90% of the cells assayed. Inhibiting

304   divisome assembly by knocking down *ftsK* almost entirely prevented the accumulation of all PG-

305   containing intermediates in *Ct* (Figs. 6E and 6F).

Discussion

The results presented here provide insight into the molecular mechanisms governing the FtsZ-less polarized cell division process of *Ct*. This study is the first to document the ordered assembly of divisome proteins in *Ct* and to investigate the roles of divisome proteins in regulating PG synthesis/organization in this obligate intracellular bacterial pathogen. Our studies showed that the divisome in *Ct* is hybrid in composition, containing elements of the divisome and elongasome from other bacteria, and a putative pathway for the assembly of the novel hybrid divisome of *Ct* is shown in Fig. 6G. Although we focused our study on a subset of the divisome and elongasome proteins that *Chlamydia* expresses (bolded in Fig. 6G), our results support our conclusion that chlamydial budding is dependent upon a hybrid divisome complex and that FtsK is required for the assembly of this hybrid divisome. At this time, we cannot rule out that other proteins act upstream of FtsK to initiate divisome assembly in this obligate intracellular bacterial pathogen.

The domain organization of FtsK is highly conserved among bacteria. The C-terminus of the protein mediates the ATP-dependent directional translocation of the protein along DNA through interaction with KOPS (Fts**K o**rienting **p**olar **s**equences) (Barre, 2001; Massey, 2006) and stimulates XerCD-dependent recombination at the *dif* site near the chromosomal terminus to decatenate chromosomal dimers that arise from homologous recombination during DNA replication to monomers (Blakely, 1993; Massey, 2006). The C-terminus of chlamydial FtsK is 41% identical to the C-terminus of *E. coli* FtsK. The N-terminus of *E. coli* FtsK encodes 4 predicted transmembrane spanning helices, which are sufficient to direct the protein to the septum in dividing cells (Yu, 1998). The N-terminus of chlamydial FtsK, which is also predicted to encode 4 transmembrane-spanning helices, is 34% identical to *E. coli* FtsK.

329   Our analyses revealed a novel spatiotemporal localization pattern of FtsK during the

330   chlamydial division process. Chlamydial FtsK forms discrete foci at the septum, foci at the

331   septum and at the base of the mother cell, or in foci only at the base of the mother cell (Figure 1).

332   Our data indicate that the foci at the base of the mother cell correspond to nascent divisome

333   complexes that form prior to the formation of a secondary bud at the base of the progenitor

334   mother cell. Our analyses further revealed there was no correlation between the stage of bud

335   formation by the initial bud (early, mid-late; Ouellette SP, 2022), and the appearance of nascent

336   divisomes at the base of the progenitor mother cell (data not shown).

337   The *Ct* divisome is hybrid in nature, containing elements of the divisome (FtsK and PBP3)

338   and elongasome (PBP2, MreB, and MreC) from other bacteria. Each of these proteins formed

339   foci at the septum, foci at the septum and at the base of the mother cell, or foci only at the base of

340   the mother cell, and the foci of each protein were restricted to one side of the MOMP-stained

341   septum (Figs. 1 and 2). Knockdown of *ftsK* using CRISPRi revealed that FtsK is necessary for

342   the assembly of this hybrid divisome complex (Fig. 4). Knockdown and inhibitor studies further

343   revealed that PBP2 is necessary for the addition of PBP3 to the divisome in *Ct* (Figs. 4 and 5).

344   The chlamydial divisome proteins all form foci in coccoid cells (Figs. 1 and 2), and FtsK

345   forms foci in dividing *Ct* that only partially overlap the distribution of PBP2, PBP3, MreC, and

346   MreB (Fig. 2 and Supp. Fig. S4A). The lack of overlap of FtsK with MreB and MreC is most

347   clearly evident in Supp. Fig. S4A, and while it is unclear why FtsK only partially overlaps the

348   distribution of the other divisome components in dividing *Ct*, MreB (Liechti 2014; Kemege

349   2015; Lee 2020) and MreC (Supp. Fig. S6A) can reorganize into rings in dividing cells, and the

350   MreC rings we detected, like PG rings (Fig. 6), were at an angle relative to the MOMP-stained

351   septum. MreC also forms rings in coccoid cells (Supp. Fig. S6B). Although MreB and MreC

352 form rings in *Ct*, we never detected FtsK rings in dividing or coccoid chlamydial cells. The

353 relevance of the angled orientation of PG and MreC rings relative to the MOMP-stained septum

354 in division intermediates is unclear. However, it appears to be a conserved feature of the cell

355 division process and may arise because the divisome proteins are often positioned slightly above

356 or below the plane of the MOMP-stained septum (Figs. 1 and 2).

357 Previous studies hypothesized that MreB filaments may substitute for FtsZ and form a

358 scaffold necessary for the assembly of the divisome in *Ct* (Ouellette SP 2012; Ouellette SP 2015;

359 Ouellette SP 2020). However, our analyses have indicated that MreB is one of the last

360 components recruited to nascent divisomes that form at the base of the mother cell in *Ct,* and

361 localization studies revealed that foci formation by FtsK, PBP2, and PBP3 are not dependent on

362 MreB filament formation (Fig. 3). Although our data indicate that MreB filaments do not form a

363 scaffold necessary for the assembly of all components of the divisome in *Ct*, MreB filaments are

364 necessary for the conversion of PG foci into PG rings in *Ct* (Fig. 6).

365 FtsZ treadmilling drives its rotational movement at the septum and this may be required for

366 the positioning of peptidoglycan biosynthetic enzymes at the division plane in gram-negative and

367 gram-positive bacteria (Bisson-Filho 2017; Yang 2017). The knockdown studies presented here

368 demonstrated that in the absence of FtsZ, chlamydial FtsK is critical for divisome assembly and

369 PG synthesis in *Ct,* and future real-time imaging studies will determine whether changes in the

370 organization/distribution of FtsK occur during chromosomal translocation and/or cell division in

371 *Chlamydia*. Furthermore, future studies will investigate the mechanisms that regulate the site of

372 assembly of nascent divisomes in the mother cell during the polarized cell division process.

373 *Ct* is a member of the Planctomycetes/Verrucomicrobia/Chlamydia superphylum and

374 members of the Chlamydia and Planctomycetes phyla do not encode FtsZ (Rivas-Marín 2016).

375   *Planctospirus limnophila* is a member of the Planctomycetes that divides by polarized budding,

376   and recent knockout studies (Rivas-Marin 2023) indicated that FtsK is the only protein of the

377   chlamydial divisome we characterized here that is essential for the growth of this free-living

378   organism. These results suggest that multiple mechanisms of FtsZ-independent polarized

379   budding have evolved in members of this superphyla. It will be of interest in future studies to

380   determine whether other members of the Planctomycetes that bud (Wiegand 2020) divide using a

381   divisome apparatus similar to *Ct*.

382   **Materials and Methods**

383   **Cell Culture**

384   HeLa cells (ATCC, Manassas, VA) were cultured in Dulbecco's Modified Eagle Medium

385   (DMEM; Invitrogen, Waltham, MA) containing 10% fetal bovine serum (FBS, Hyclone, Logan,

386   UT) at 37°C in a humidified chamber with 5% CO_2. HeLa cells were infected with *Ct* serovar L2

387   434/Bu in the same media. Infections of HeLa cells with chlamydial transformants were

388   performed in DMEM containing 10% FBS and 0.36 U/mL penicillin G (Sigma-Aldrich).

389   **Cloning**

390   The plasmids and primers used for generating mCherry fusions of FtsK, PBP2, PBP3,

391   and MreC are listed in Supp. Table S1. The chlamydial *ftsK*, *pbp2, pbp3,* and *mreC* genes were

392   amplified by PCR with Phusion DNA polymerase (NEB, Ipswich, MA) using 10

393   ng *C. trachomatis* serovar L2 genomic DNA as a template. The PCR products were purified

394   using a PCR purification kit (Qiagen) and inserted into the pBOMB4-Tet (-GFP) plasmid, which

395   confers resistance to β-lactam antibiotics. The plasmid was cut at the NotI (FtsK-mCherry) or the

396   KpnI (mCherry-PBP2, mCherry-PBP3, mCherry-MreC) site, and the chlamydial genes were

397   inserted into the cut plasmid using the HiFi DNA Assembly kit (NEB) according to the

398   manufacturer's instructions. The products of the HiFi reaction were transformed into NEB-

399   5αI�q competent cells (NEB) and transformants were selected by growth on plates containing

400   ampicillin. DNA from individual colonies was isolated using a mini-prep DNA isolation kit

401   (Qiagen), and plasmids were initially characterized by restriction digestion to verify the inserts

402   were the correct size. Clones containing inserts of the correct size were DNA sequenced prior to

403   use.

404   **DNA and RNA purification and RT-qPCR**

405   Total nucleic acids were extracted from HeLa cells infected with *Ct* plated in 6-well dishes as

406   described previously (Ouellette 2015, Ouellette, Blay et al. 2021). For RNA isolation, cells were

407   rinsed one time with PBS, then lysed with 1mL Trizol (Invitrogen) per well. Total RNA was

408   extracted from the aqueous layer after mixing with 200μL per sample of chloroform following

409   the manufacturer's instructions. Total RNA was precipitated with isopropanol and treated with

410   DNase (Ambion) according to the manufacturer's guidelines prior to cDNA synthesis using

411   SuperScript III (Invitrogen). For DNA, infected cells were rinsed one time with PBS, trypsinized

412   and pelleted before resuspending each pellet in 500μL of PBS. Each sample was split in half, and

413   genomic DNA was isolated from each duplicate sample using the DNeasy extraction kit

414   (Qiagen) according to the manufacturer's guidelines. Quantitative PCR was used to measure

415   *C. trachomatis* genomic DNA (gDNA) levels using an *euo* primer set. 150ng of each sample was

416   used in 25μL reactions using standard amplification cycles on a QuantStudio3 thermal cycler

417   (Applied Biosystems) followed by a melting curve analysis. *ftsK, pbp2, euo*, and *omcB* transcript

418   levels were determined by RT-qPCR using SYBR Green as described previously (Ouellette SP

419   2021) (see Supp. Table S2 for primers used for measuring gDNA levels and RT-qPCR).

420   Transcript levels were normalized to genomes and expressed as ng cDNA/gDNA.

Transformation of *Ct*

421   *Ct* was transformed as described previously (Wang 2011). Briefly, HeLa cells were plated in a 10cm plate at a density of 5×10^6 cells the day before beginning the transformation procedure. *Ct* lacking its endogenous plasmid (-pL2) was incubated with 10μg of plasmid DNA in Tris-CaCl$_2$ buffer (10 mM Tris-Cl pH 7.5, 50 mM CaCl$_2$) for 30 min at room temperature. HeLa cells were trypsinized, washed with 8mL of 1x DPBS (Gibco), and pelleted. The pellet was resuspended in 300μL of the Tris-CaCl$_2$ buffer. *Ct* was mixed with the HeLa cells and incubated at room temperature for an additional 20 min. The mixture was added to 10mL of DMEM containing 10% FBS and 10 μg/mL gentamicin and transferred to a 10cm plate. At 48hpi, the HeLa cells were harvested and *Ct* in the population were used to infect a new HeLa cell monolayer in media containing 0.36 U/ml of penicillin G to select for transformants. The plate was incubated at 37°C for 48 hours. These harvest and re-infection steps were repeated every 48hrs until inclusions were observed.

Immunofluorescence Microscopy

435   HeLa cells were seeded in 10cm plates at a density of 5×10^6 cells per well the day before the infection. *Ct* L2 or chlamydial strains transformed with plasmids encoding FtsK-mCherry, mCherry-PBP2, mCherry-PBP3, or mCherry-MreC or with plasmids that direct the constitutive expression of the crRNAs targeting the *pbp2* or *ftsK* promoters were used to infect HeLa cells in DMEM. For experiments with the transformants, aTc was added to the media of infected cells at the indicated concentration and time. At 21hpi, cells were detached from the 10cm plate by scraping and pelleted by centrifugation for 30 seconds. The pellet was resuspended in 1 mL of 0.1x PBS (Gibco) and transferred to a 2mL tube containing 0.5mm glass beads (ThermoFisher Scientific). Cells were vortexed for 3 mins. then centrifuged at 800rpm for 2 mins. in a

444   microfuge. 20μLs of the supernatant was mixed with 20μLs of 2x fixing solution (6.4%

445   formaldehyde and 0.044% glutaraldehyde) and incubated on a glass slide for 10 min at room

446   temperature. Cells were washed with 3 times with PBS, and the cells were permeabilized by

447   incubation with PBS containing 0.1% Triton X-100 for 1 min. Cells were washed with PBS two

448   times. For experiments with *Ct* L2, the cells were incubated with a goat primary antibody against

449   the major outer-membrane protein (MOMP; Meridian, Memphis, TN), and the mouse primary

450   antibody that recognizes endogenous FtsK raised against recombinant CT739 protein

451   (**https://doi.org/10.1099/mic.0.047746-0**), or with rabbit antibodies raised against peptides

452   derived from PBP 2 or PBP3 (Ouellette SP 2012) . Briefly, chlamydial antigens or peptides

453   emulsified with Freund's incomplete adjuvant were used to immunize animals via intramuscular

454   injections three times with an interval of 2 weeks. Antisera were collected from the immunized

455   animals 2 to 4 weeks after the final immunization as the primary antibodies. After the primary

456   antibody labeling, the cells were then rinsed with PBS and incubated with donkey anti-goat IgG

457   (Alexa 488) and donkey anti-mouse IgG (Alexa 594) or donkey-anti-rabbit IgG (Alexa 594)

458   secondary antibodies (Invitrogen). Experiments in which we visualized the distribution of the

459   various mCherry fusions, the localization of the mCherry fluorescence was compared to the

460   distribution of MOMP. In some experiments, we determined the distribution of the MreB_6x His

461   fusion by staining cells expressing the fusion with a rabbit anti-6x His antibody (Abcam,

462   Cambridge, MA) and the goat anti-MOMP antibody followed by the appropriate secondary

463   antibodies. Cells were imaged using Zeiss AxioImager2 microscope equipped with a 100x oil

464   immersion PlanApochromat objective and a CCD camera. During image acquisition, 0.3μm xy-

465   slices were collected that extended above and below the cell. The images were collected such

466   that the brightest spot in the image was saturated. The images were deconvolved using the

467   nearest neighbor algorithm in the Zeiss Axiovision 4.7 software. Deconvolved images were

468   viewed and assembled using Zeiss Zen-Blue software. For each experiment, three independent

469   replicates were performed, and the values shown for localization are the average of the 3

470   experiments. In some instances, 3D projections of the acquired xy slices were generated using

471   the Zeiss Zen-Blue software.

472   **Peptidoglycan (PG) labeling**

473   PG was labeled by incubating cells with 4mM ethylene-D-alanine-D-alanine (E-DA-DA) as

474   described (Cox 2020). The incorporated E-DA-DA was fluorescently labeled using the Click &

475   Go^{TM} labeling kit (Vector Laboratories). The distribution of fluorescently labeled PG was

476   compared to the distribution of MOMP and endogenous FtsK or the distribution of mCherry-

477   PBP3. Three independent replicates were performed, and the values shown are the average of the

478   3 experiments.

479   **Inclusion forming unit assay**

480   HeLa cells were infected with *Ct* (-pL2) transformed with the pBOMB4 Tet (-GFP) plasmid

481   encoding the indicated aTc-inducible gene. At 8hpi, aTc was added to the culture media at the

482   indicated concentration. Control cells were not induced. At 48hpi, the HeLa cells were dislodged

483   from the culture dishes by scraping and collected by centrifugation. The pellet was resuspended

484   in 1 mL of 0.1x PBS (Gibco) and transferred to a 2mL tube containing 0.5mm glass bead tubes

485   (ThermoFisher Scientific). Cells were vortexed for 3 min. followed by centrifugation at 800rpm

486   for 2 min. The supernatants were mixed with an equal volume of a 2x sucrose-phosphate (2SP)

487   solution (ref) and frozen at -80°C. At the time of the secondary infection, the chlamydiae were

488   thawed on ice and vortexed. Cell debris was pelleted by centrifugation for 5 min at 1k x g at 4°C.

489   The EBs in the resulting supernatant were serially diluted and used to infect a monolayer of

490   HeLa cells in a 24-well plate. The secondary infections were allowed to grow at 37°C for 24 hrs

491   before they were fixed and labeled for immunofluorescence microscopy by incubating with a

492   goat anti-MOMP antibody followed by a secondary donkey anti-goat antibody (Alexa Fluor

493   594). The cells were rinsed in PBS and inclusions were imaged using an EVOS imaging system

494   (Invitrogen). The number of inclusions were counted in 5 fields of view and averaged. Three

495   independent replicates were performed, and the values from the replicates were averaged to

496   determine the number of inclusion forming units. Chi-squared analysis was used to compare

497   IFUs in induced and uninduced samples.

498   **Effect of A22 and mecillinam on the profile of division intermediates and on PG and**

499   **divisome protein localization in *Ct***

500   HeLa cells were infected with *Ct* transformed with the pBOMB4-Tet (-GFP) plasmid

501   encoding FtsK-mCherry, mCherry-PBP2, mCherry-PBP3, mCherry-MreC, or MreB-6xHis. The

502   fusions were induced at 20hpi with 10nM aTc for 1hr in the absence or presence of 75 μM A22.

503   At 22hpi, cells were harvested and prepared for staining as described above. Three independent

504   replicates were performed, and the values shown for localization are the average of the 3

505   experiments.

506   HeLa cells were infected with *Ct* L2 and 20μM mecillinam (Sigma) was added to the media

507   of infected cells at 17 hpi. Control cells were untreated. At 22 hpi, infected cells were harvested

508   and RBs were prepared and stained with MOMP, FtsK, PBP2 or PBP3 antibodies as described

509   above. Alternatively, cells were incubated with 4mM EDA-DA at 17hpi in the presence or

510   absence of 20μM mecillinam. The cells were harvested at 22hpi, and RBs were prepared and PG

511   was click-labeled, and its distribution was visualized in MOMP-stained cells as described above.

512   Three independent replicates were performed, and the values shown for localization are the

513   average of the 3 experiments.

514   **Immunoblotting**

515   HeLa cells infected with *Ct* L2 were harvested by scraping the infected cells from the plate at

516   24hpi. Uninfected HeLa cells were included as a control. The HeLa cells were pelleted by

517   centrifugation, resuspended in SDS sample buffer and electrophoresed on a 10% SDS

518   polyacrylamide gel. The gel was electrophoretically transferred to nitrocellulose (Schleicher and

519   Schuell), and the filter was incubated with mouse polyclonal antibodies raised against

520   chlamydial FtsK. The filter was rinsed and incubated with 800 donkey anti-mouse IgG secondary

521   antibodies (LICOR, Lincoln, NE) and imaged using a LICOR Odyssey imaging system.

522   HeLa cells were infected with *Ct* transformed with plasmids that inducibly express FtsK-

523   mCherry, mCherry-PBP2, mCherry-PBP3, or mCherry-MreC. The fusions were induced by the

524   addition of 10nM aTc to the media of infected cells at 17hpi. The cells were harvested and

525   pelleted at 21hpi. The cell pellet was resuspended in 1 mL of 0.1x PBS (Gibco) and transferred

526   to a 2mL tube containing 0.5mm glass beads (ThermoFisher Scientific). Cells were vortexed for

527   3 min. followed by centrifugation at 800rpm for 2 min. The supernatant was collected and

528   centrifuged for 3 min at 13,000 rpm and the pellet containing *Ct* was resuspended in TBS

529   containing 1% TX-100, 1X protease inhibitor cocktail (Sigma), and 5μM lactacystin. The

530   suspension was sonicated 3 times on ice and centrifuged at 13,000 rpm for 3 mins. The

531   supernatant was collected and mixed with SDS sample buffer. The samples were boiled and

532   electrophoresed on a 10% SDS polyacrylamide gel, and the gel was electrophoretically

533   transferred to nitrocellulose. The blots from these analyses were probed with a rabbit anti-

534   mCherry primary antibody (Invitrogen) and a 800 donkey anti-rabbit IgG secondary antibodies

535   (LICOR, Lincoln, NE). The filters were imaged using a LICOR Odyssey imaging system.

536   HeLa cells were infected with *Ct* transformed with the pBOMB4-Tet (-GFP) plasmid

537   encoding mCherry-PBP2 or mCherry-PBP3. The fusions were induced with 10nM aTc at 17hpi.

538   Uninduced cells were included as a control. The cells were harvested at 21hpi, and samples were

539   processed for immunoblotting as described above. The blots were probed with rabbit polyclonal

540   antibodies raised against peptides derived from chlamydial PBP2 or PBP3 (Ouellette SP 2012).

541   The blots were then rinsed and incubated with 800 donkey anti-rabbit IgG secondary antibodies

542   (LICOR, Lincoln, NE). The filters were imaged using a LICOR Odyssey imaging system.

543   **ACKNOWLEDGMENTS**

548

549   **Figure Legends**

550   **Figure 1:**(A) The linear divisome assembly pathway of *E. coli* is shown. *Ct* encodes the

551   divisome proteins boxed in red. HeLa cells were infected with *Ct* L2 and RBs were prepared at

552   21hpi. The cells were fixed and stained with MOMP (green) and FtsK (red) antibodies. The

553   distribution of FtsK in (B) coccoid cells and in (C) cell division intermediates that had not

554   initiated secondary bud formation is shown. Bars are 1 μm. HeLa cells were infected with *Ct*

555   transformed with the pBOMB4 -Tet (-GFP) plasmid encoding FtsK-mCherry. The fusion was

556   induced with 10nM aTc for 1 hr. and RBs were prepared from infected HeLa cells at 21hpi and

557   stained with MOMP antibodies (green). The distribution of MOMP relative to the mCherry

558   fluorescence (D) in coccoid cells and in (E) cell division intermediates that had not initiated

559   secondary bud formation is shown. Bars are 1μm. Arrowheads in C and E denote foci of FtsK

560   above or below the MOMP-stained septum. (F) HeLa cells were infected with *Ct* L2. At 21hpi,

561   the cells were harvested and RBs were stained with MOMP antibodies. The number of dividing

562   cells that had initiated secondary bud formation was quantified in 150 cells. Three independent

563   replicates were performed, and the values shown are the average of the 3 replicates. (G)

564   Endogenous FtsK and FtsK-mCherry accumulate in foci at the septum of secondary buds

565   (marked with arrowheads).

566   **Figure 2:** HeLa cells were infected with *Ct* transformed with PBP2, PBP3, or MreC with an N-

567   terminal mCherry tag, or with *Ct* transformed with an MreB_6xHis fusion (Lee 2020). Each of

568   the fusions was induced by adding 10nM aTc to the media at 17hpi. Lysates were prepared at

569   21hpi and the cells were fixed and stained with a MOMP antibody. The distribution of the

570   mCherry fluorescence in (A) coccoid cells and in (B) dividing cells that had not initiated

571   secondary bud formation is shown. Cells expressing the MreB_6xHis fusion were stained with

572   rabbit anti-6x His antibody (red) and MOMP antibodies (green). Dividing cells with foci at the

573   septum, foci at the septum and foci at the base of the mother cell, or foci at the base alone are

574   shown for each of the fusions. Arrowheads in B denote foci of the divisome proteins above or

575   below the plane of the MOMP-stained septum. (C) HeLa cells were infected with *Ct* L2.

576   Alternatively, cells were infected with *Ct* that were transformed with FtsK-mCherry, mCherry-

577   PBP2, mCherry-PBP3, mCherry-MreC, or MreB_6xHis. The cells expressing the fusions were

578   induced with aTc for 1.5hrs then fixed at 21hpi and the distribution of endogenous FtsK, or the

579   mCherry fluorescence in cells inducibly expressing the mCherry fusions, or the distribution of

580   MreB in cells where the MreB_6xHis fusion was inducibly expressed was quantified. A small

581   fraction (2 %) of dividing cells contained multiple foci of each of the divisome proteins at the

582   septum and/or the base of the cell. Since these cells were relatively rare, we included these cells

583   with cells that contained a single foci in the quantification. The localization profiles were

584   quantified in 100 cells. Three independent replicates were performed, and the values shown are

585   the average of the 3 replicates. Chi-squared analysis revealed that the localization profiles of

586   endogenous FtsK and FtsK-mCherry are not statistically different from each other, but they are

587   statistically different than the PBP2, PBP3, MreC and MreB localization profiles (* – p<0.009).

588   The localization profile of the MreB fusion is also statistically different than the localization

589   profiles of the mCherry fusions of PBP2 and PBP3 (#- p = 0.05). (D) Hela cells were infected

590   with *Ct* transformed with PBP2, PBP3, or MreC with a N-terminal mCherry tag, or with *Ct*

591   transformed with an MreB_6xHis fusion (Lee 2020). The fusions were induced by adding 10 nM

592   aTc to the media at 17hpi. The cells were harvested at 21hpi and *Ct* were harvested and stained

593   with FtsK and MOMP antibodies. The cells expressing the MreB fusion were stained with FtsK,

594   MOMP, and 6xHis antibodies. Imaging analyses revealed that FtsK was present in foci at the

595   septum and in foci at the base in these cells, while each of the fusions was only detected at the

596   septum where they overlapped the distribution of septal FtsK (Bars are1μm).

597   **Figure 3:** (A) HeLa cells infected with *Ct* L2 were treated with 75μM A22 for 1 hour. Control

598   cells were not treated with A22. Lysates were prepared at 21hpi and the number of coccoid and

599   dividing cells in the population were quantified in 100 cells. Three independent replicates were

600   performed, and the values shown are the average of the 3 replicates. (B-E) Alternatively, HeLa

601   cells were infected with *Ct* transformed with plasmids encoding FtsK-mCherry, mCherry-PBP2,

602   mCherry-PBP3, mCherry-MreC, or MreB-6xHis. The fusions were induced at 20hpi with 10nM

603   aTc for 1hr in the absence (B and D) or presence (C and E) of 75µM A22. Coccoid cells

604   prepared from the infected cells at 21hpi were stained with MOMP antibodies (green). The

605   MreB-6xHis fusion was also stained with 6xHis antibodies (red). Panel B shows the distribution

606   of the fusions in untreated coccoid cells. Panel C illustrates the effect of A22 on the localization

607   of the fusions in coccoid cells. Bars in B and C are 1µm. The distribution of FtsK-mCherry,

608   mCherry-PBP2, mCherry-PBP3, mCherry-MreC, and MreB-6xHis was quantified in (D) control

609   coccoid cells and in (E) A22-treated cells coccoid cells (n=50) is shown. Three replicates were

610   performed, and the values shown in D and E are the averages of the 3 replicates. Student T-test

611   indicated that A22 had a statistically significant effect on the localization of MreB and MreC (* –

612   p<0.01).

613   **Figure 4:** HeLa cells were infected with *Ct* transformed with the pBOMBL-12CRia plasmid,

614   which constitutively expresses a *ftsK* crRNA or *pbp2* crRNA and encodes dCas12 under the

615   control of an aTc-inducible promoter. dCas12 was induced at 17hpi by adding 5nM aTc to the

616   media. In a control infection, the expression of dCas12 was not induced. Cells were harvested at

617   24hpi and the morphology of *Ct* in induced and uninduced control cells was assessed in 250

618   cells. 3 replicates were performed, and the values shown are the averages of the 3 replicates (A

619   and B). The localization of endogenous FtsK, endogenous PBP2, and endogenous PBP3 was

620   assessed in cells transformed with the pBOMBL-12CRia plasmid that targets *ftsK* or *pbp2*. The

621   localization is shown in coccoid cells where dCas12 expression was (C) uninduced or (D)

622   induced. White bars are 1µm. (E and F) The localization profiles of FtsK, PBP2, and PBP3 were

623   quantified in uninduced and induced cells. 3 replicates were performed, and the values shown are

624   the averages of the 3 replicates.

625 **Figure 5:** Effect of mecillinam on endogenous FtsK, PBP2, and PBP3 localization. (A) HeLa

626 cells were infected with *Ct* and 20μM mecillinam was added to the media at 17hpi. Untreated

627 coccoid cells were included as a control. The cells were harvested at 21hpi and the morphology

628 of MOMP-stained cell was assessed in 200 cells. 3 replicates were performed, and the values

629 shown are the averages of the 3 replicates. (B and C) The localization of endogenous FtsK,

630 endogenous PBP2, and endogenous PBP3 in untreated coccoid or in mecillinam-treated coccoid

631 cells is shown. Bars are1μM. (D and E) Localization of FtsK, PBP2, and PBP3 in untreated and

632 mecillinam-treated coccoid cells was quantified in 50 cells. Three replicates were performed, and

633 the values shown are the averages of the 3 replicates.

634 **Figure 6:** PG distribution in *Ct*. HeLa cells were infected with *Ct* L2. At 17hpi, 4mM ethylene-

635 DA-DA (EDA-DA) was added to the media, the cells were harvested at 21hpi, and the EDA-DA

636 was click labeled and compared to the distribution of MOMP. (A) Imaging analyses revealed

637 that PG formed foci at the septum and at the base in some dividing cells. (B) Imaging analyses

638 revealed that PG organization at the septum and at the base of some dividing cells differed. In

639 this example, a PG foci was detected at the septum and a PG ring was detected at the base of a

640 dividing cell. (C) The localization of click-labeled PG was compared to the localization of

641 endogenous FtsK and mCherry-PBP3 at the septum of dividing cells. 3D projections revealed

642 that multiple foci of each protein are associated with PG intermediates. Cartoons are included to

643 assist the reader in visualizing the angled orientation of PG relative to the MOMP-stained septum

644 in the dividing cells. (D) PG organization in untreated coccoid cells. (E) Quantification of PG

645 organization in untreated coccoid cells, A22-treated coccoid cells, mecillinam-treated coccoid

646 cells, and in coccoid cells resulting from the inducible knockdown of *ftsk*. Fifty cells were

647 counted for each condition. Three replicates were performed and the average from the 3

648   replicates is shown. (F) PG organization in A22-treated and mecillinam-treated coccoid cells, and

649   in coccoid cells resulting from the inducible knockdown of *ftsk* is shown. Bars are 1μm. (G)

650   Putative *Ct* divisome assembly pathway is shown. Proteins characterized in this study are bolded.

651   The ordering of the remaining proteins is based on the assembly of the divisome and elongasome

652   in *E. col*i (Du 2017; Liu 2020).

653   **Supp. Fig. S1:**(A) Lysates were prepared from uninfected HeLa cells and HeLa cells infected

654   with *Ct* L2. At 21hpi, lysates were prepared and characterized by immunoblotting with FtsK-

655   specific antibodies. (B) HeLa cells were infected with *Ct* transformed with the various mCherry

656   fusions used in this study; FtsK-mCherry (molecular mass - 114,664 Da), mCherry-PBP2

657   (molecular mass - 150,842 Da), mCherry-PBP3 (molecular mass - 100,150 Da), or mCherry-

658   MreC (molecular mass - 63,906 Da). The fusions were induced with 10nM aTc at 17hpi. HeLa

659   cells were harvested at 21hpi and lysates were prepared and characterized by immunoblotting

660   analysis with a rabbit polyclonal mCherry antibodies. (C) HeLa cells were infected with *Ct*

661   transformed N-terminal fusions of PBP2 or PBP3. The fusions were induced (+aTc) at17hpi.

662   Controls were not induced (-aTc). The cells were harvested at 21hpi and lysates were prepared as

663   described in the Methods and characterized by immunoblotting analysis with rabbit antibodies

664   raised against peptides derived from chlamydial PBP2 or PBP3. The PBP3 antibody primarily

665   detects a single species with the predicted molecular mass of mCherry-PBP3 in the induced

666   sample. The PBP2 antibody primarily detects a species of ~120kD in the induced sample, which

667   is smaller than the predicted molecular mass of mCherry-PBP2 (~150kD). The failure to detect

668   full length mCherry-PBP2 may be due to the masking of the epitope recognized by the PBP2

669   antibody by the N-terminal mCherry tag in the full-length protein. (D) HeLa cells were infected

670   with *Ct* transformed with mCherry-PBP2 or mCherry-PBP3. The fusions were induced by the

671   addition of 10nM aTc to the media of the infected cells at 19hpi. Infected cells were harvested at

672   21hpi and lysates were prepared and stained with the PBP2 or PBP3 antibodies. The staining

673   with the PBP2 and PBP3 antibodies completely overlaps the mCherry fluorescence from the

674   mCherry-PBP2 and mCherry-PBP3 fusions (Bars are 3µm)

675   **Supp. Fig. S2:** (A) HeLa cells were infected with *Ct* transformed with FtsK-mCherry, mCherry-

676   PBP2, mCherry-PBP3, and mCherry-MreC. The fusions were uninduced or induced by the

677   addition of varying amounts of aTc to the media of the infected cells at 8hpi. The cells were

678   harvested at 48hpi and *Ct* were isolated. The number of infectious *Ct* in the lysates was measured

679   by an IFU assay. Chi-squared analysis revealed that induction of the fusions did not have a

680   statistically significant effect on the growth of *Ct* and the production of infectious EBs. (B) Each

681   of the mCherry fusions accumulate in foci at the septum and in foci at the base (marked with

682   arrowheads) of dividing cells with secondary buds.

683   **Supp. Fig. S3: (A)** Localization analyses with rabbit polyclonal antibodies that recognize

684   endogenous PBP2 or PBP3. These analyses revealed that endogenous PBP2 and PBP3

685   accumulate in foci in coccoid cells, and in foci at the septum, foci at the septum and base, or in

686   foci at the base alone in cell division intermediates in *Ct*. PBP2 and PBP3 foci are also detected

687   at the base of secondary buds. Bars are1µm (B) Quantification revealed that the localization

688   profiles of endogenous PBP2 and PBP3 were not statistically different than the localization

689   profiles of the mCherry-PBP2 and mCherry-PBP3 fusions shown in Fig. 2C.

690   **Supp. Fig. S4:** HeLa cells were infected with *Ct* transformed with PBP2, PBP3, or MreC with an

691   N-terminal mCherry tag, or with *Ct* transformed with an MreB_6xHis fusion (Lee 2020). Each of

692   the fusions was induced by adding 10nM aTc to the media at 17hpi. Lysates were prepared at

693   21hpi and the cells were fixed and stained with a MOMP antibody. The distribution of the

694   mCherry fluorescence in dividing cells that had not initiated secondary bud formation is shown.

695   Cells expressing the MreB_6xHis fusion were stained with rabbit anti-6xHis antibody (red) and

696   MOMP antibodies (green). In the dividing cells shown there are (A) foci of the fusions at the

697   septum and at the base of the mother cell or foci at the base of the mother cell only that overlap

698   the distribution of FtsK. Bars are1μm (B) The percentage of dividing cells in which the fusions

699   overlapped the distribution of FtsK at the septum, at the septum and at the base, and at the base

700   alone was quantified in 100 cells. Three independent replicates were performed and the values

701   shown are the average of the 3 replicates.

702   **Supp. Fig. S5:** HeLa cells were infected with *Ct* transformed with the pBOMBL12CRia

703   plasmid that constitutively expresses *ftsK* or *pbp2*-targeting crRNAs. dCas12 expression was

704   induced by the addition of 5nM aTc to the media of infected cells at 8hpi. Control cells were not

705   induced. Nucleic acids were isolated from induced cells and from uninduced controls at various

706   times post-infection, and RT-qPCR was used to measure *ftsK* or *pbp2* transcript levels. (A) The

707   induction of dCas12 resulted in ~10-fold reduction in *ftsK* transcript levels in cells expressing the

708   *ftsK*-targeting crRNA, (B) and ~8-fold reduction in *pbp2* transcript levels in cells expressing the

709   *pbp2*-targeting crRNA, while these crRNAs had minimal or no effect on chlamydial *euo* and

710   *omcB* transcript levels. HeLa cells were infected with *Ct* transformed pBOMBL12CRia plasmid

711   that constitutively expresses a (C) *ftsK* or (D) *pbp2*-targeting crRNA. dCas12 expression was

712   induced by the addition of 5nM aTc to the media of infected cells at 8hpi. Control cells were not

713   induced. The infected cells were fixed at 24hpi and stained with MOMP and Cas12 antibodies.

714   *Ct* morphology was normal and dCas12 was undetectable in the inclusions of uninduced control

715   cells. Foci of dCas12 were observed in induced cells, and *Ct* in the inclusion exhibited an

716   enlarged aberrant morphology. Bars in C and D are 2μm. (E) HeLa cells were infected with *Ct*

717   transformed with the pBOMBL12CRia plasmid that constitutively expresses a *ftsK* or *pbp2*-

718   targeting crRNA. dCas12 was induced at 17hpi by the addition of 10nM aTc to the media.

719   Control cells were not induced. The cells were harvested at 21hpi, and *Ct* were prepared and

720   stained with antibodies that recognize that endogenous FtsK or PBP2. Quantification shows that

721   polarized foci of FtsK and PBP2 were almost undetectable when *ftsK* or *pbp2* were transiently

722   knocked down.

723   **Supp. Fig. S6**. MreC rings in (A) dividing *Ct* and in (B) coccoid *Ct*. Bars are1μm.

724   **Supp. Table S1** List of primers and plasmids used for cloning mCherry fusions of FtsK, PBP2,

725   PBP3, MreB and MreC.

726   **Supp. Table S2**: List of primers used for RT-qPCR.

727   **References:**

728   **Abdelrahman, Y., Ouellette, Scot P., Belland, Robert J., Cox, John V. (2016). "Polarized**

729   **Cell Division of Chlmaydia Trachomatis " <u>PLOS Pathogens</u>**

730   **+**

731   **Abdelrahman, Y. M. and R. J. Belland (2005). "The chlamydial developmental cycle."**

732   **<u>FEMS Microbiol Rev</u> 29(5): 949-959.**

733

734   **Abdelrahman, Y. O., Scot P. Belland, Robert J. Cox, John V. (2016). "Polarized Cell**

735   **Division of Chlamydia trachomatis." <u>PLOS Pathogens</u>.**

736

737   **F. Barre, B. Søballe, B. Michel, M. Aroyo, M. Robertson, D. Sherratt, Circles: The**

738   **replication-recombination-chromosome segregation connection, Proc. Natl. Acad. Sci.**

739   **U.S.A. 98 (15) 8189-8195, https://doi.org/10.1073/pnas.111008998 (2001).**

740

741   Barrows, J. M. and E. D. Goley (2021). "FtsZ dynamics in bacterial division: What, how,

742   and why?" Curr Opin Cell Biol 68: 163-172.

743

744   Bean, G. J., S. T. Flickinger, W. M. Westler, M. E. McCully, D. Sept, D. B. Weibel and K.

745   J. Amann (2009). "A22 disrupts the bacterial actin cytoskeleton by directly binding and

746   inducing a low-affinity state in MreB." Biochemistry 48(22): 4852-4857.

747

748   Bisson-Filho, A. W., Y. P. Hsu, G. R. Squyres, E. Kuru, F. Wu, C. Jukes, Y. Sun, C.

749   Dekker, S. Holden, M. S. VanNieuwenhze, Y. V. Brun and E. C. Garner (2017).

750   "Treadmilling by FtsZ filaments drives peptidoglycan synthesis and bacterial cell

751   division." Science 355(6326): 739-743.

752

753   Blakely, G., May, G., McCulloch, R., Arciszewska, L. K., Burke, M., Lovett, S. T., &

754   Sherratt, D. J. (1993). Two related recombinases are required for site-specific

755   recombination at dif and cer in E. coli K12. Cell, 75(2), 351–361.

756   https://doi.org/10.1016/0092-8674(93)80076-q

757

758   Cox, J. V. A., Yasser Mohamed. Ouellette, Scot P. (2020). "Penicillin-binding proteins

759   regulate multiple steps in the polarized cell division process of Chlamydia." Nature

760   Du, S. L., Joe (2017). "Assembly and activation of the Escherichia coli divisome."

761   Molecular Microbiology.

762

763   GW, L. (2021). "Localized Peptidoglycan Biosynthesis in Chlamydia trachomatis

764   Conforms to the Polarized Division and Cell Size Reduction Developmental Models." **Front**

765   **Microbiol**.

766

767   Kaur, H. and A. M. Lynn (2022). "Mapping the FtsQBL divisome components in bacterial

768   NTD pathogens as potential drug targets." **Front Genet** 13: 1010870.

769

770   Kemege, K. E., J. M. Hickey, M. L. Barta, J. Wickstrum, N. Balwalli, S. Lovell, K. P.

771   Battaile and P. S. Hefty (2015). "Chlamydia trachomatis protein CT009 is a structural and

772   functional homolog to the key morphogenesis component RodZ and interacts with division

773   septal plane localized MreB." **Mol Microbiol** 95(3): 365-382.

774

775   Kocaoglu, O., H. C. Tsui, M. E. Winkler and E. E. Carlson (2015). "Profiling of β-lactam

776   selectivity for penicillin-binding proteins in Streptococcus pneumoniae D39." **Antimicrob**

777   **Agents Chemother** 59(6): 3548-3555.

778

779   Lee, J., Cox, John V., Ouellette, Scot P. (2020). "Critical Role for the Extended N Terminus

780   of Chlmaydial MreB in Directing Its Membrane Association and Potential Interaction with

781   Divisome Proteins " **Journal of Bacteriology** 202.

782

783   Lee, J. K., G. A. Enciso, D. Boassa, C. N. Chander, T. H. Lou, S. S. Pairawan, M. C. Guo,

784   F. Y. M. Wan, M. H. Ellisman, C. Sütterlin and M. Tan (2018). "Replication-dependent

785   **size reduction precedes differentiation in Chlamydia trachomatis." Nature**

786   **Communications 9(1): 45.**

787

788   **Liechti, G., E. Kuru, M. Packiam, Y. P. Hsu, S. Tekkam, E. Hall, J. T. Rittichier, M.**

789   **VanNieuwenhze, Y. V. Brun and A. T. Maurelli (2016). "Pathogenic Chlamydia Lack a**

790   **Classical Sacculus but Synthesize a Narrow, Mid-cell Peptidoglycan Ring, Regulated by**

791   **MreB, for Cell Division." PLoS Pathog 12(5): e1005590.**

792

793   **Liechti, G. W., E. Kuru, E. Hall, A. Kalinda, Y. V. Brun, M. VanNieuwenhze and A. T.**

794   **Maurelli (2014). "A new metabolic cell-wall labelling method reveals peptidoglycan in**

795   **Chlamydia trachomatis." Nature 506(7489): 507-510.**

796

797   **Liu, X. B., Jacob. Consoli, Elisa. Vollmer, Waldemar. Blaauwen, Tanneke den. (2020).**

798   **"MreC and MreD balance the interaction between the elongasome proteins PBP2 and**

799   **RodA." PLOS Genetics.**

800

801   **Massey, T. H., Mercogliano, C. P., Yates, J., Sherratt, D. J., & Löwe, J. (2006). Double-**

802   **stranded DNA translocation: structure and mechanism of hexameric FtsK.** *Molecular*

803   *cell*, *23*(4), 457–469. https://doi.org/10.1016/j.molcel.2006.06.019

804

805   **Ouellette, S. P., E. A. Blay, N. D. Hatch and L. A. Fisher-Marvin (2021). "CRISPR**

806   **Interference To Inducibly Repress Gene Expression in Chlamydia trachomatis." Infect**

807   **Immun 89(7): e0010821.**

808

809 **Ouellette SP, F.-M. L., Harpring M, Lee J, Rucks EA, Cox JV (2022). "Localized**

810 **cardiolipin synthesis is required for the assembly of MreB during the polarized cell division**

811 **of Chlamydia trachomatis." <u>PLOS Pathogens</u>.**

812

813 **Ouellette SP, K. G., Subtil A, Ladant D. (2012). "Chlamydia co-opts the rod shape-**

814 **determining proteins MreB and Pbp2 for cell division." <u>Mol Microbiol</u>.**

815

816 **Ouellette, S. P., K. J. Rueden, Y. M. AbdelRahman, J. V. Cox and R. J. Belland (2015).**

817 **"Identification and Partial Characterization of Potential FtsL and FtsQ Homologs of**

818 **Chlamydia." <u>Front Microbiol</u> 6: 1264.**

819

820 **Ouellette, S. P., K. J. Rueden, E. Gauliard, L. Persons, P. A. de Boer and D. Ladant (2014).**

821 **"Analysis of MreB interactors in Chlamydia reveals a RodZ homolog but fails to detect an**

822 **interaction with MraY." <u>Front Microbiol</u> 5: 279.**

823

824 **Ouellette, S. P. L., Junghoon. Cox, John V. (2020). "Division without Binary Fission: Cell**

825 **Division in the FtsZ-Less Chlamydia." <u>Journal of Bacteriology</u>.**

826

827 **Ouellette, S. P. R., Kelsey J. AbdelRahman, Yasser M. Cox, John V. Belland, Robert J.**

828 **(2015). "Identification and Partial Characterization of Potential FtsL and FtsQ Homologs**

829 **of Chlamydia." <u>Frontiers in Microbiology</u>.**

830

831   Rivas-Marín, E., I. Canosa, E. Santero and D. P. Devos (2016). "Development of Genetic

832   Tools for the Manipulation of the Planctomycetes." Front Microbiol 7: 914.

833

834   Rivas-Marin, E., D. Moyano-Palazuelo, V. Henriques, E. Merino and D. P. Devos (2023).

835   "Essential gene complement of Planctopirus limnophila from the bacterial phylum

836   Planctomycetes." Nat Commun 14(1): 7224.

837

838   Stephens, C. (1998). "Bacterial sporulation: a question of commitment?" Curr Biol 8(2):

839   R45-48.

840

841   Veiga, H. and M. G. Pinho (2017). "Staphylococcus aureus requires at least one

842   FtsK/SpoIIIE protein for correct chromosome segregation." Mol Microbiol 103(3): 504-

843   517.

844

845   Wang, T. J., P. Gona, M. G. Larson, G. H. Tofler, D. Levy, C. Newton-Cheh, P. F. Jacques,

846   N. Rifai, J. Selhub, S. J. Robins, E. J. Benjamin, R. B. D'Agostino and R. S. Vasan (2006).

847   "Multiple biomarkers for the prediction of first major cardiovascular events and death." N

848   Engl J Med 355(25): 2631-2639.

849

850   Wang, Y., S. Kahane, L. T. Cutcliffe, R. J. Skilton, P. R. Lambden and I. N. Clarke (2011).

851   "Development of a transformation system for Chlamydia trachomatis: restoration of

852   glycogen biosynthesis by acquisition of a plasmid shuttle vector." PLoS Pathog 7(9):

853   e1002258.

854

855 Wiegand, S., M. Jogler, C. Boedeker, D. Pinto, J. Vollmers, E. Rivas-Marín, T. Kohn, S. H.

856 Peeters, A. Heuer, P. Rast, S. Oberbeckmann, B. Bunk, O. Jeske, A. Meyerdierks, J. E.

857 Storesund, N. Kallscheuer, S. Lücker, O. M. Lage, T. Pohl, B. J. Merkel, P. Hornburger, R.

858 W. Müller, F. Brümmer, M. Labrenz, A. M. Spormann, H. J. M. Op den Camp, J.

859 Overmann, R. Amann, M. S. M. Jetten, T. Mascher, M. H. Medema, D. P. Devos, A. K.

860 Kaster, L. Øvreås, M. Rohde, M. Y. Galperin and C. Jogler (2020). "Cultivation and

861 functional characterization of 79 planctomycetes uncovers their unique biology." Nat

862 Microbiol 5(1): 126-140.

863

864 Yang, X., Z. Lyu, A. Miguel, R. McQuillen, K. C. Huang and J. Xiao (2017). "GTPase

865 activity-coupled treadmilling of the bacterial tubulin FtsZ organizes septal cell wall

866 synthesis." Science 355(6326): 744-747.

867

868 Yu, X. C., A. H. Tran, Q. Sun and W. Margolin (1998). "Localization of cell division

869 protein FtsK to the Escherichia coli septum and identification of a potential N-terminal

870 targeting domain." J Bacteriol 180(5): 1296-1304.

871

872

Figure 1
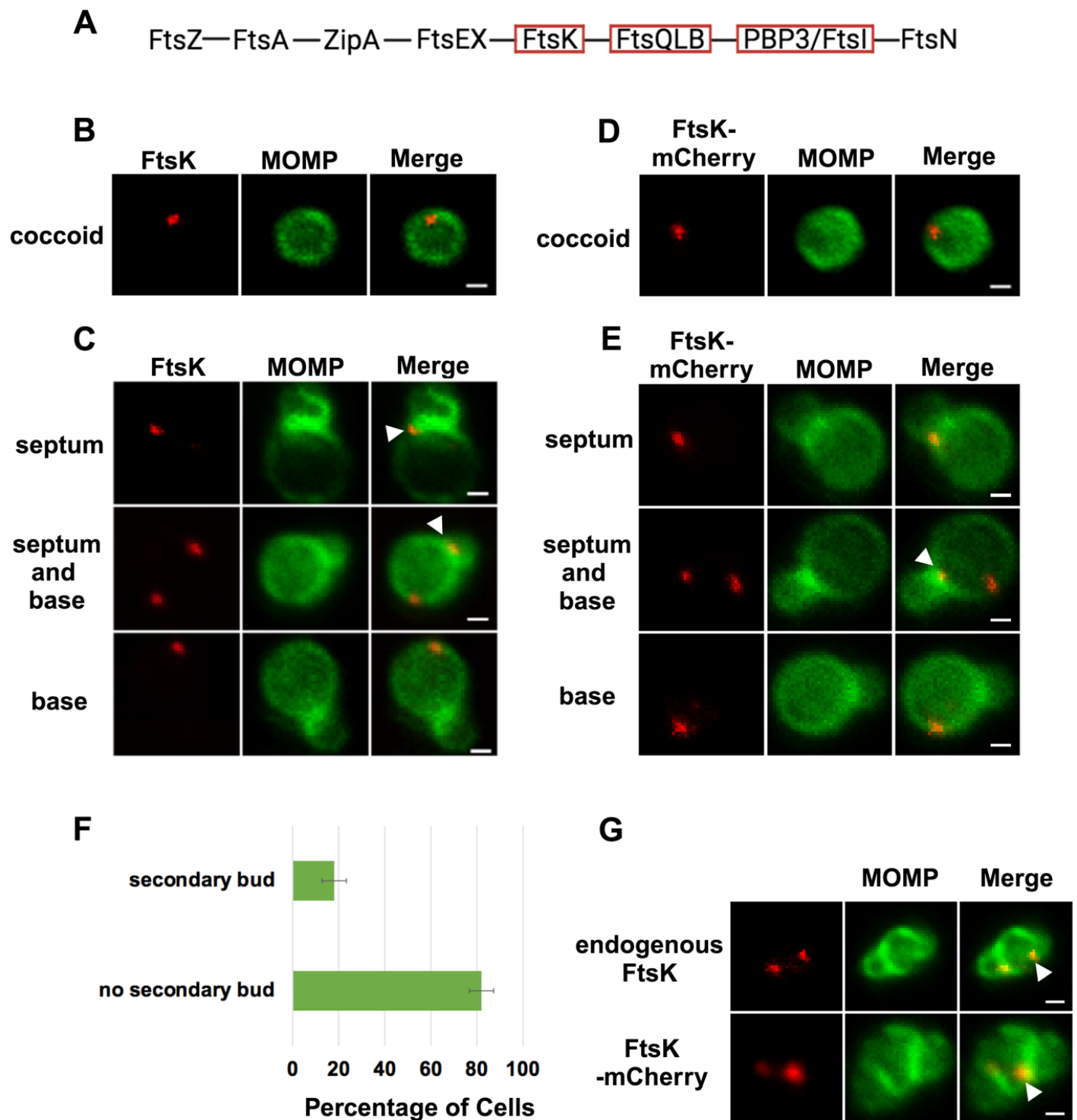
Figure 2
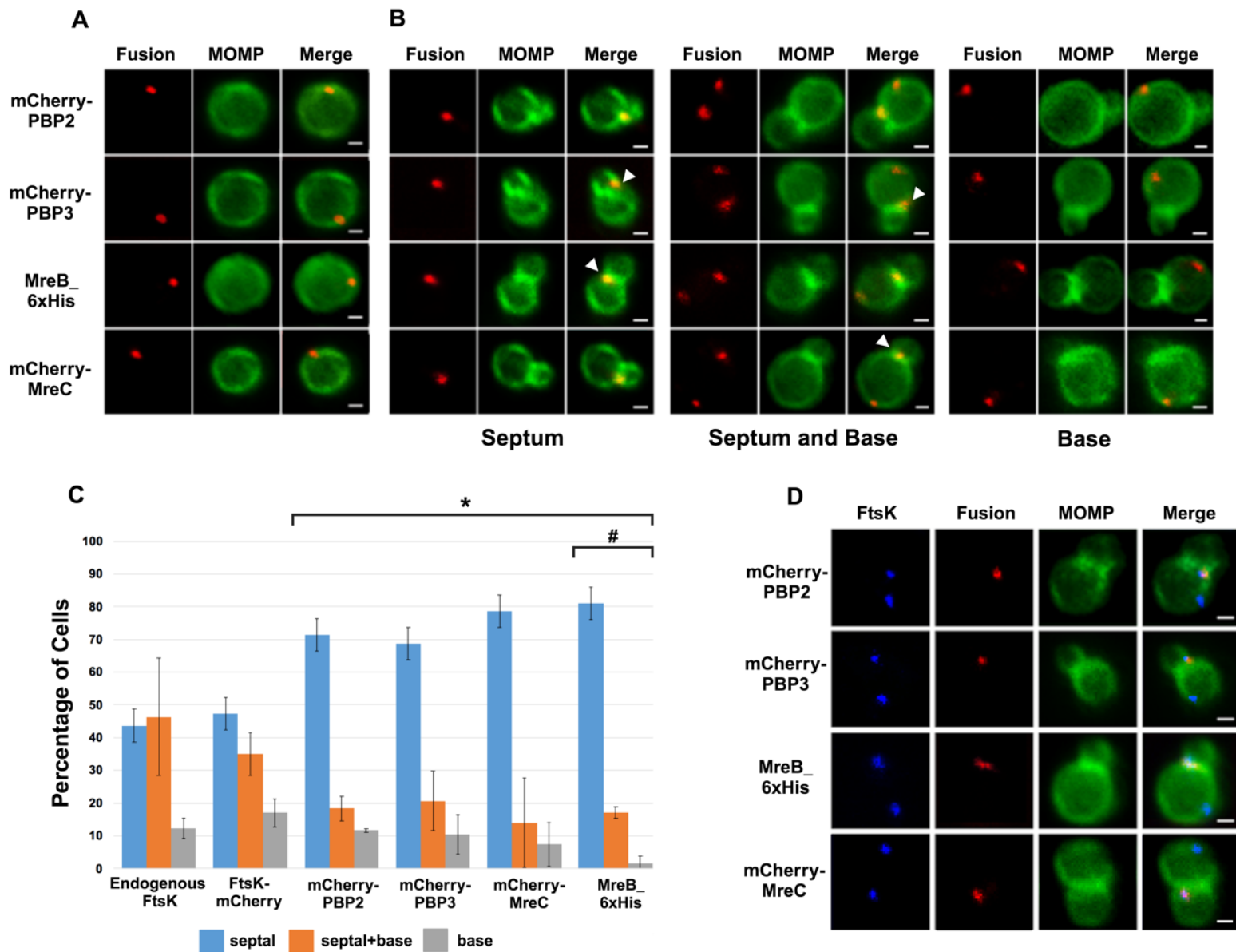
Figure 3
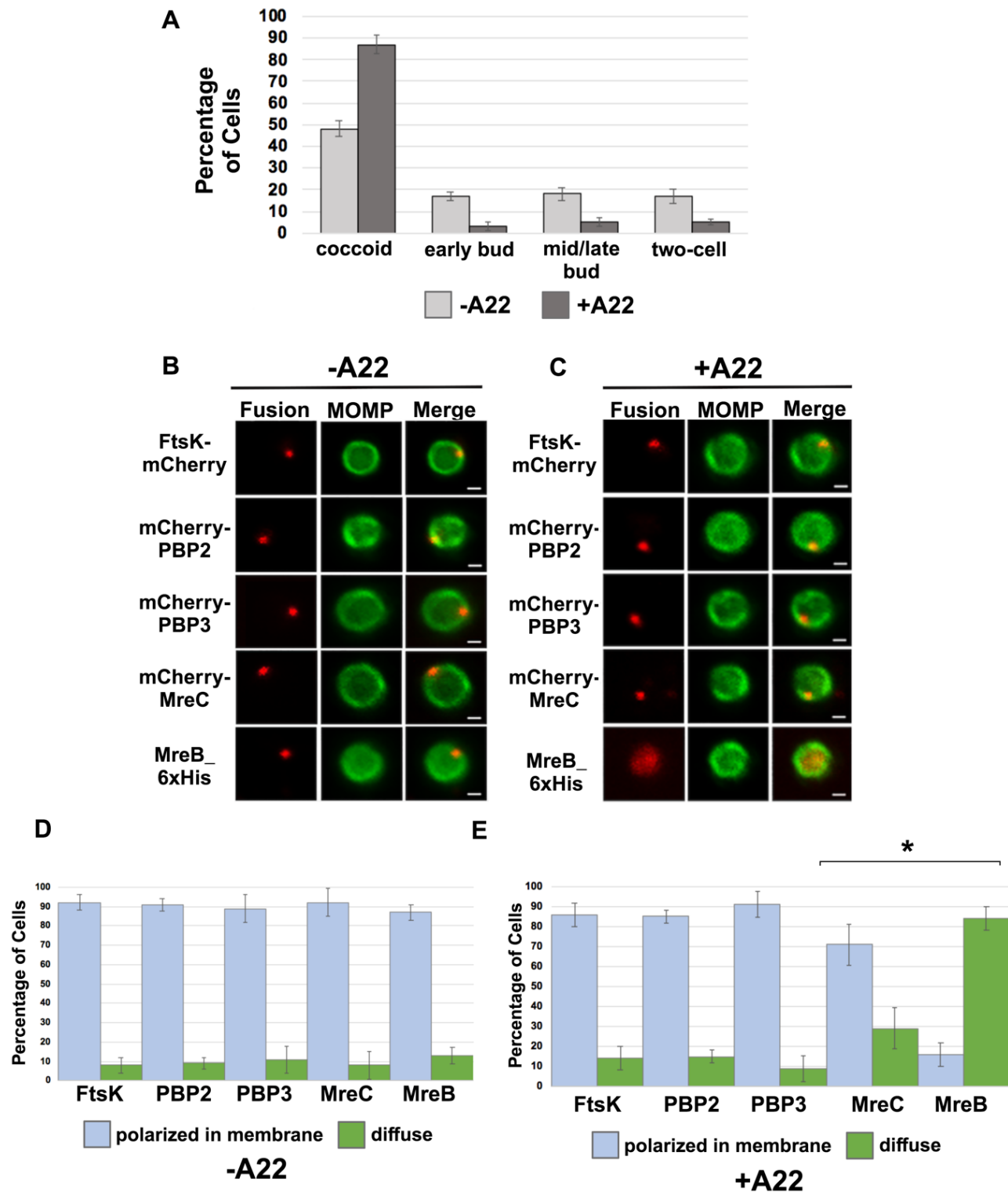
Figure 4
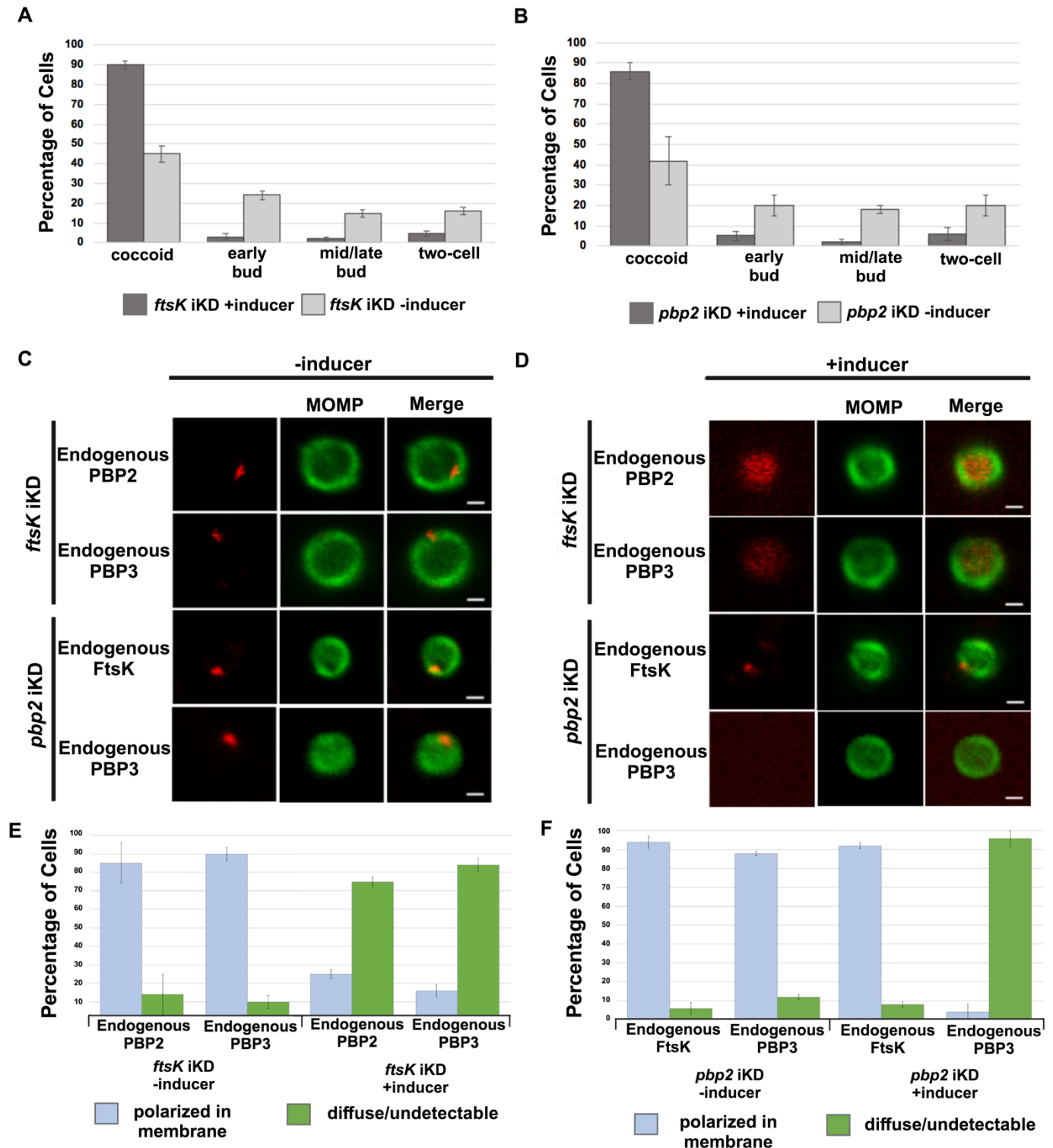
Figure 5

Figure 6

Supp. Figure S1

A

kD · *Ct* · - · +
250
150
100
50
37
25
10

FtsK Antibody

B

kD
250
150
100
50

FtsK-mCherry Lysate · mCherry-PBP2 Lysate · mCherry-PBP3 Lysate · mCherry-MreC Lysate

C

kD · aTc · - · +
250
150
100
75
50
37
25
10

mCherry PBP2 Lysate: PBP2 Antibody

kD · aTc · - · +
250
150
100
75
50
37
25
10

mCherry PBP3 Lysate: PBP3 Antibody

D

PBP2 Antibody · mCherry-PBP2 · MOMP · Merge

PBP3 Antibody · mCherry-PBP3 · MOMP · Merge

Supp. Figure S2

A

B
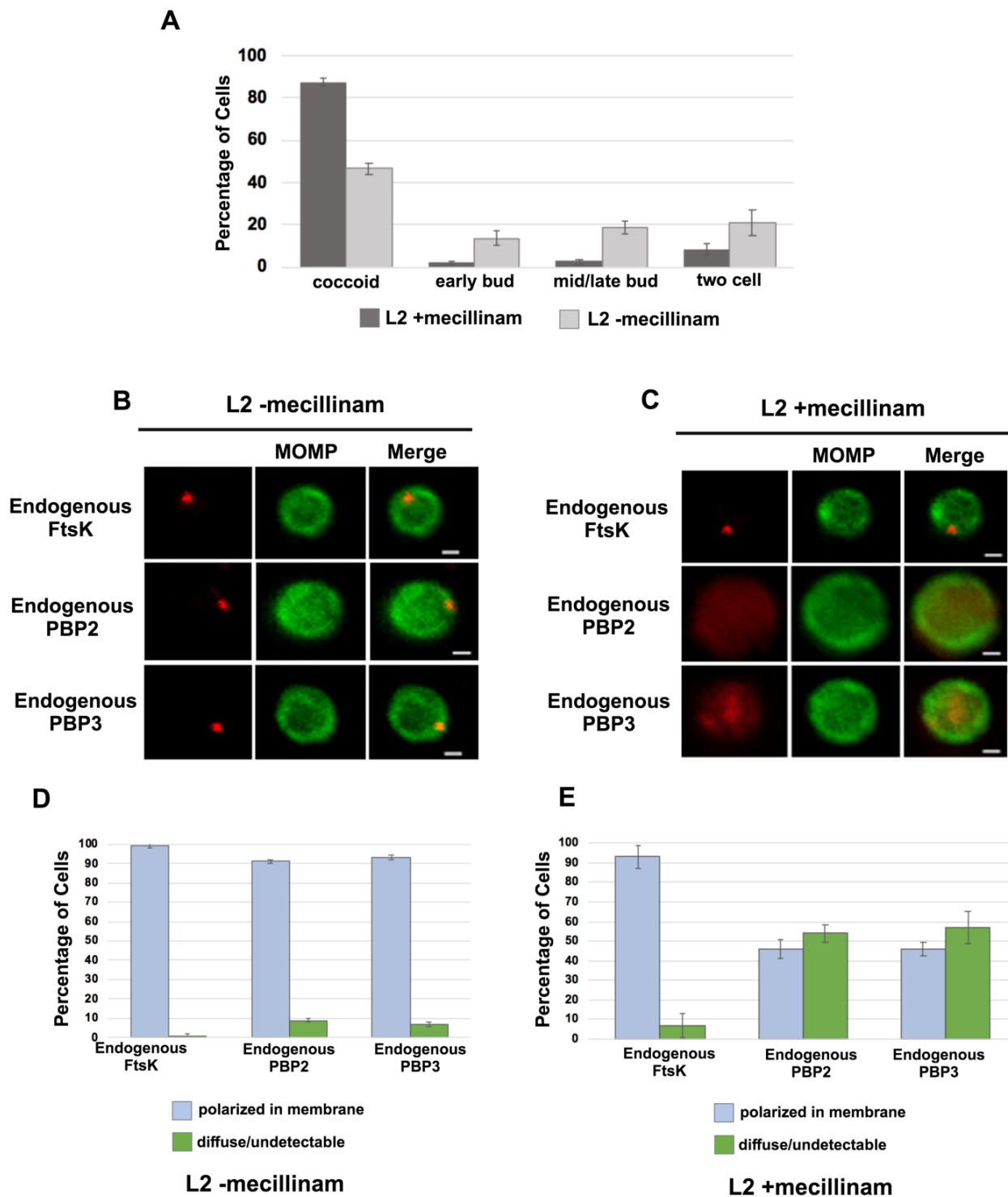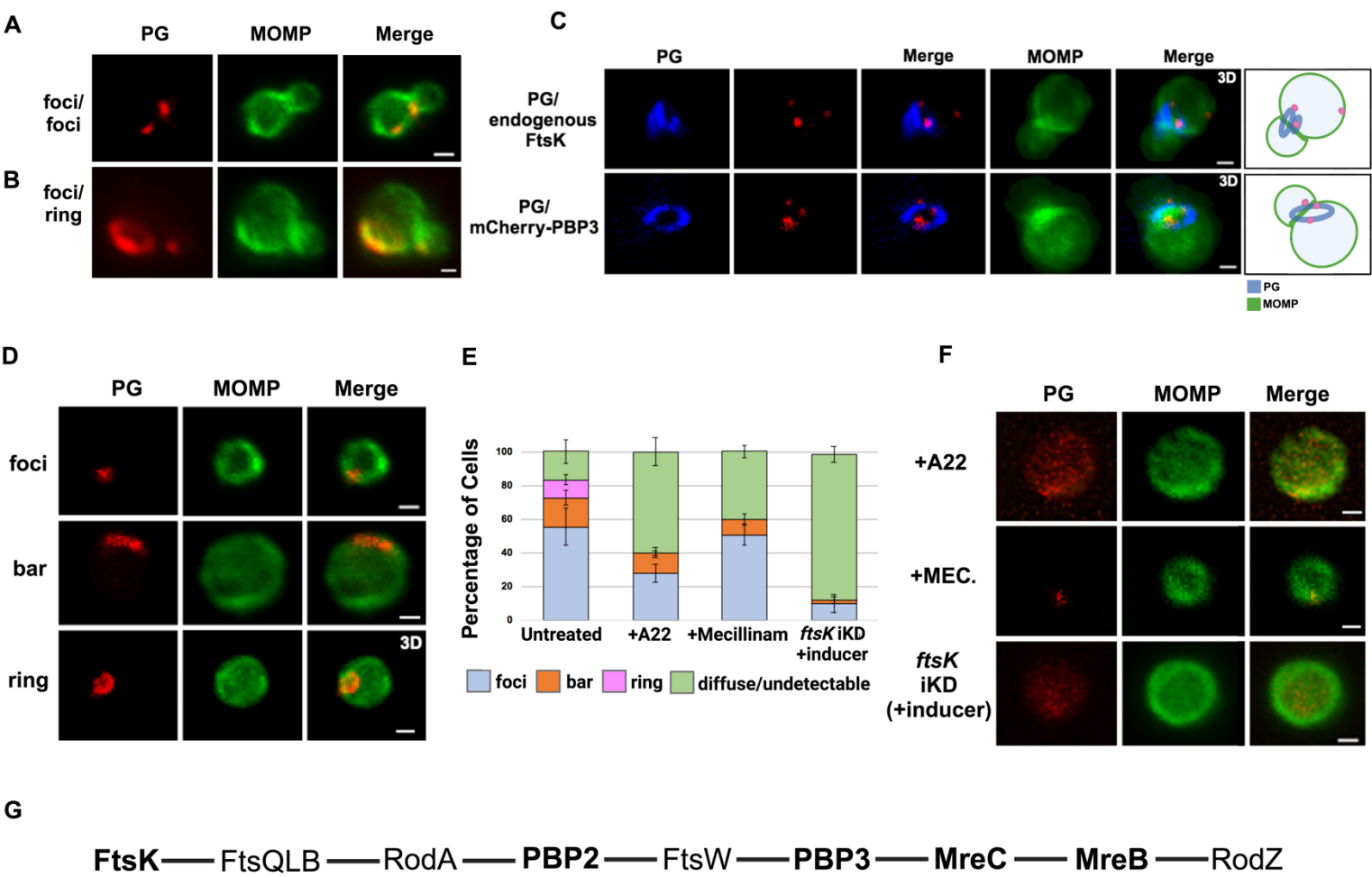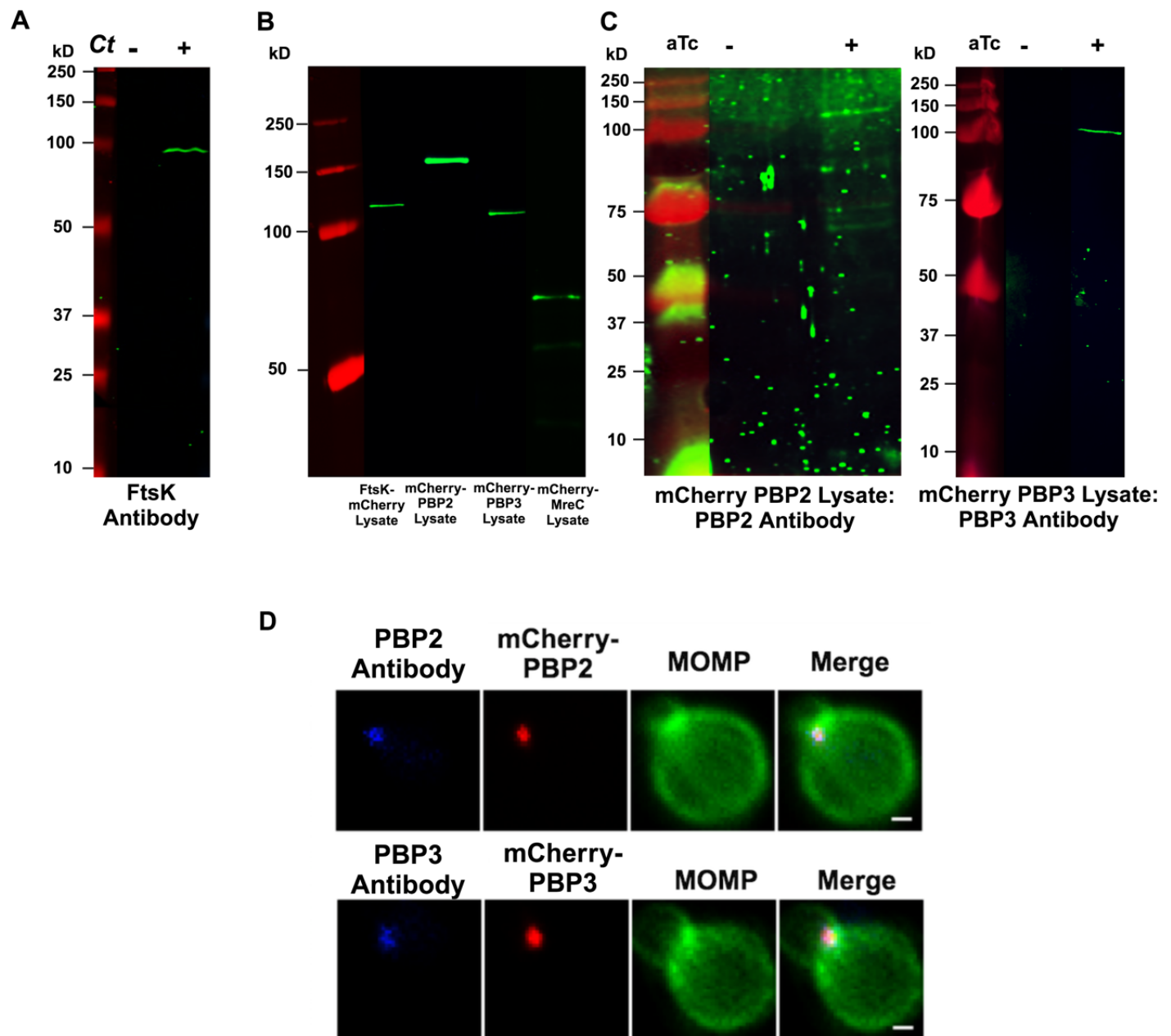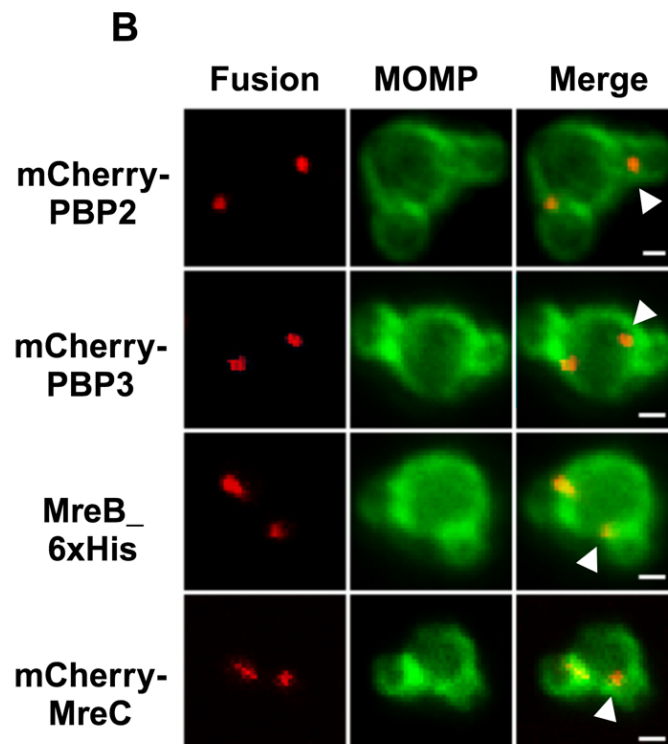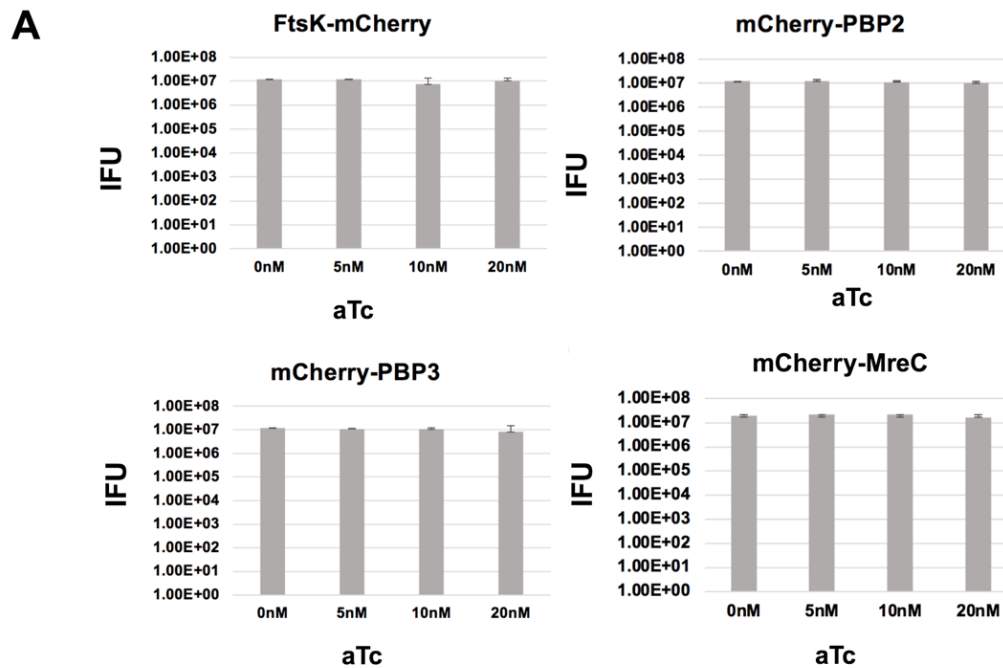
Supp. Figure S3

A

B

Supp. Figure S4

A

Overlaps FtsK at the septum and base

Overlaps FtsK at the base
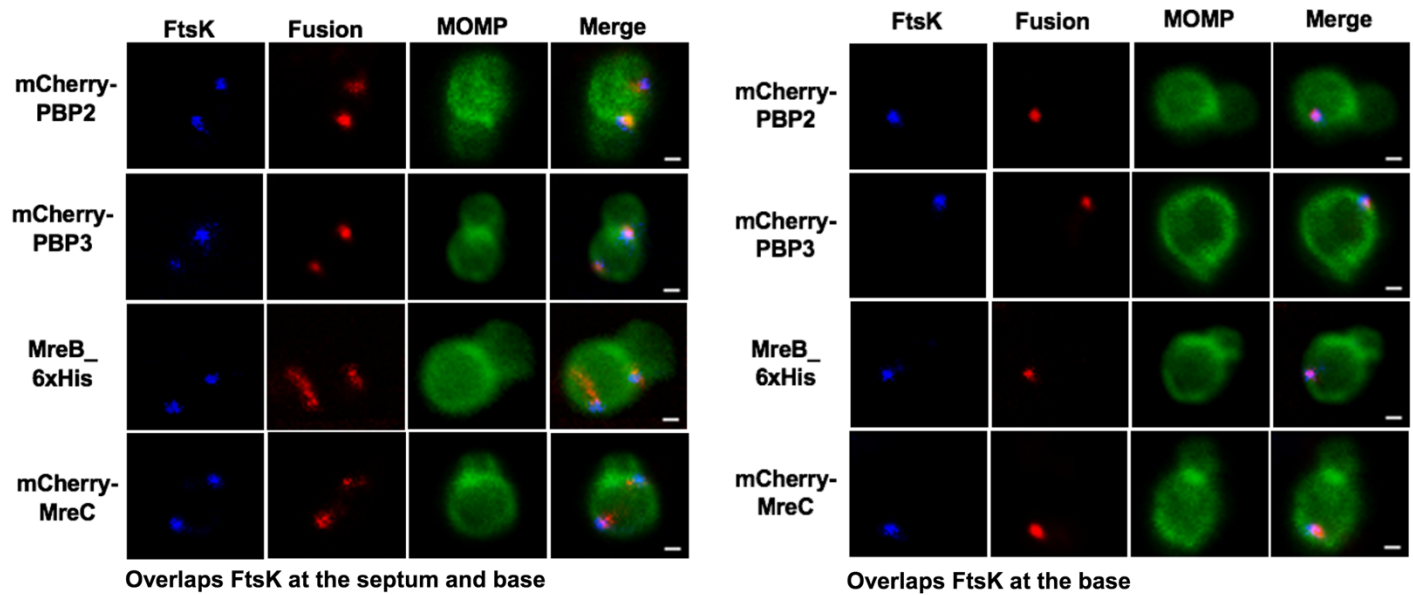
B
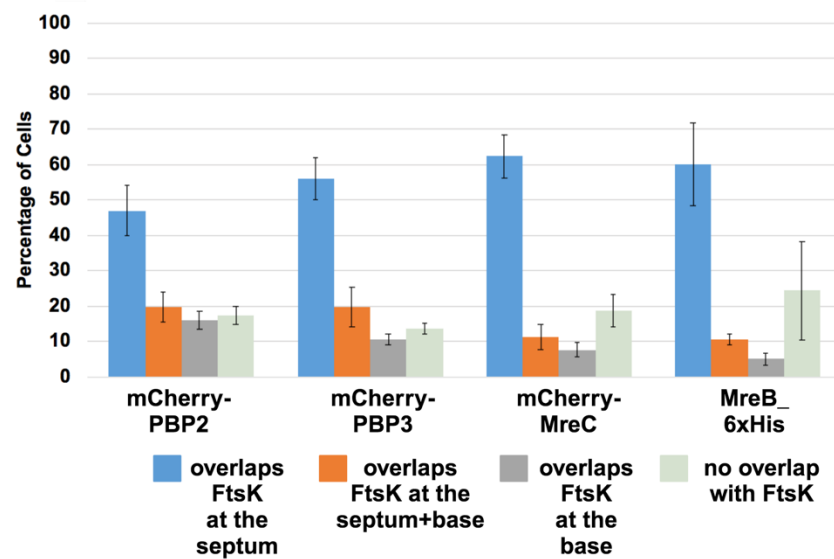
Supp. Figure S5

A
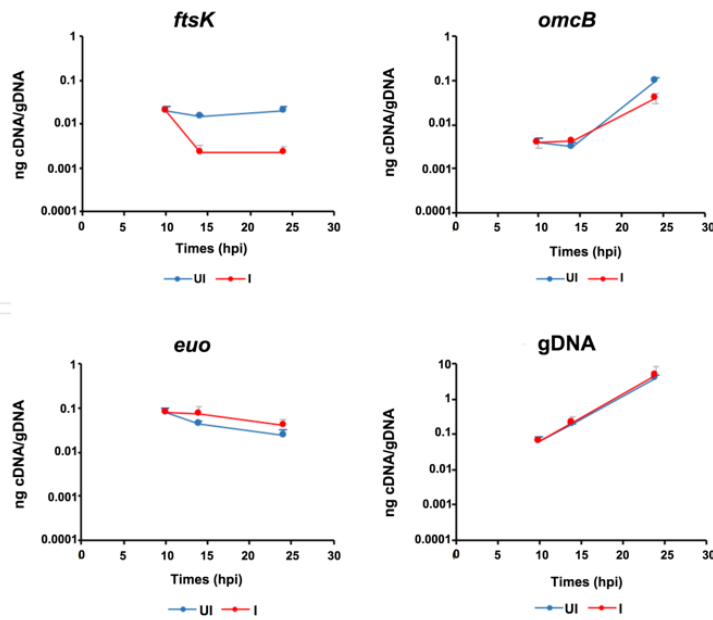
B

C

D

E
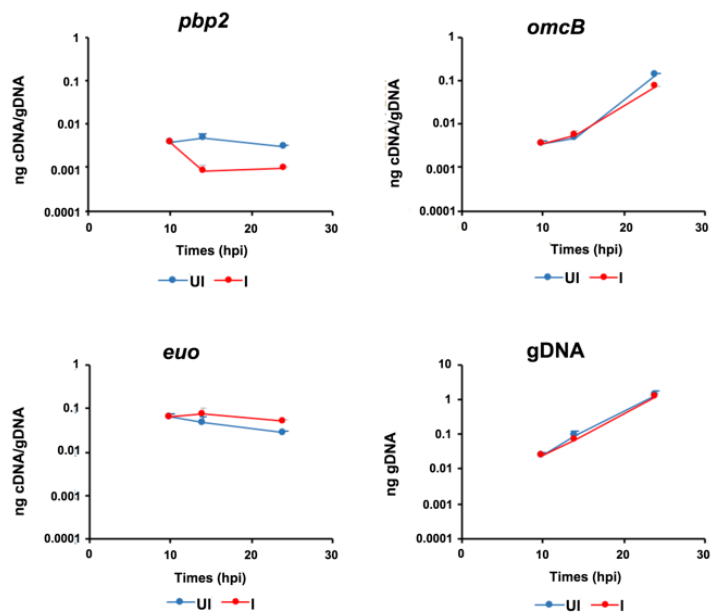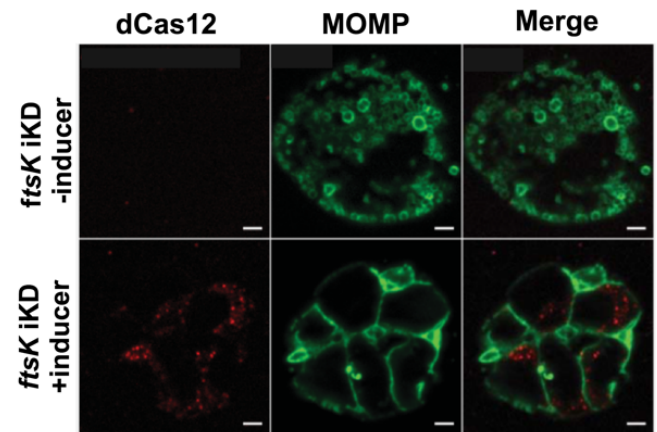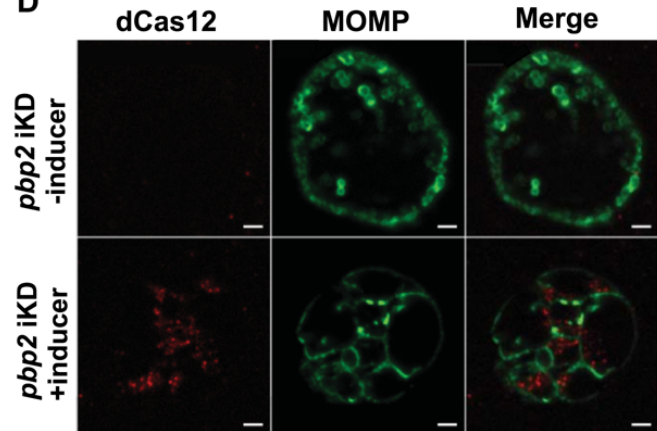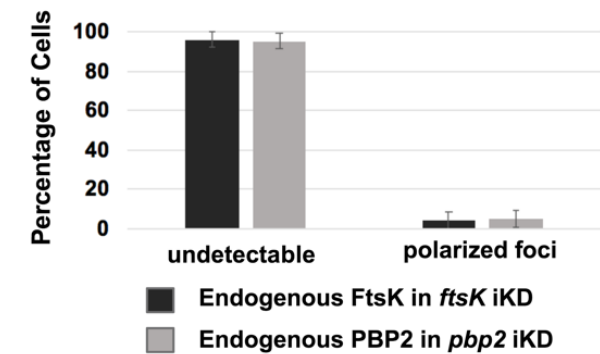
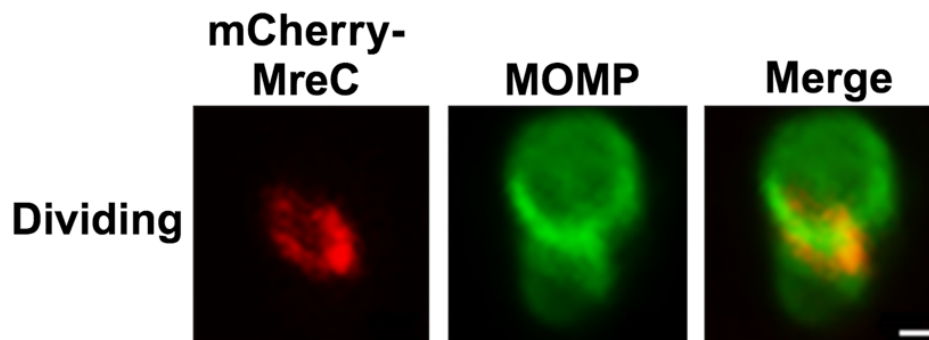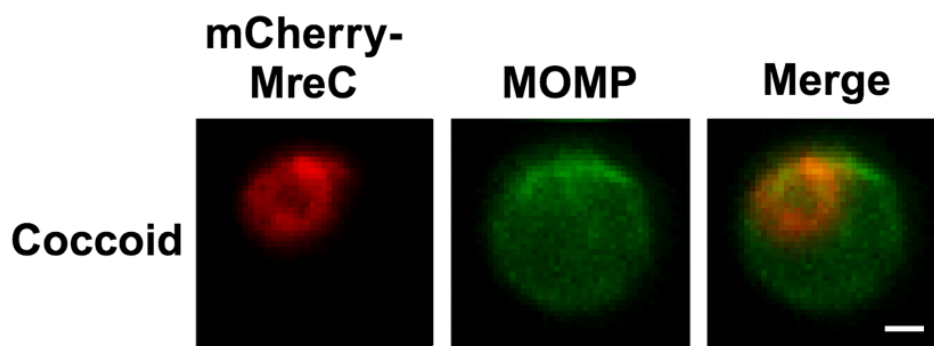**Supp. Figure S6**

Supp. Table S1

Primer Name	Primer Sequence (5'-3')	GC content (%)	TM (°C)
FtsK_mCherry (fwd)	AGAGGAGAAAGGATCTGCGGCCGCATGGGAAAAGAACGGAAGAAAGCAAG	52	72.8
FtsK_mCherry (rvs)	CCCTTAGAGACCATTGCGGCCGCATCGTCCTGATTTGATAATTGGACTAGTATTTGAC	47	72.4
mCherry_PBP2 (fwd)	ATGGTCTCTAAGGGCGAGGAAGAC	54	59.1
mCherry_PBP2 (rvs)	ATGGTCGACCGGTACCTTAGCTGAAAGATTTTTTACGAATCTCTTCCCATTTCTCTATC	41	70.2
mCherry_PBP3 (fwd)	ATGGTCTCTAAGGGCGAGGAAGAC	54	59.1
mCherry_PBP3 (rvs)	ATGGTCGACCGGTACCCTATTTGCGATTCCATTCCTCATATAGCAG	48	69.9
mCherry_MreC (fwd)	ATGGTCTCTAAGGGCGAGGAAGAC	54	59.1
mCherry_MreC (rvs)	ATGGTCGACCGGTACCCTACTCCCAAATCAAACCAAAAATATCAGGACG	47	70.4
Plasmid	pBOMB4-tet		

Supp. Table S2

Primer Name	Primer Sequence (5'-3')	GC content (%)	TM (°C)
ftsK (fwd)	CGACTCCAAGTTCCTCTTCTTC	39.1	55.2
ftsK (rvs)	GATCCAGTGGTTCCTGCAATA	47.6	54.6
pbp2 (fwd)	TAACACTGACGCGGAACATAG	47.6	55.1
pbp2 (rvs)	CCGAAAGCATGAGCAGATAGA	47.6	54.8
omcB (fwd)	CGGTAGGATCTCCCTATCCTATT	47.8	54.4
omcB (rvs)	CGAACTCTGCTTCACATGGTA	47.6	55
euo (fwd)	CGAAGACTACTCGTTGGGAAATA	43.5	54.7
euo (rvs)	AACAGAAGCTCTCCTTGATAAGT	39.1	53.8